IIETA International Information and Engineering Technology Association
Advancing the World of Information and Engineering

Journal of New Materials for Electrochemical Systems
Vol. 28, No. 1, January 2025, pp 1-23
Journal homepage: http://iieta.org/journals/jnmes

Optimization of Comfort and Saturated Magnetic and Electromagnetic Properties of Polyester Fabric Impregnated with Silica/Kaolinite/Silver In-Situ to Protect the Human Body

Ehsan Zarinabadi[1,2], Ramin Abghari[2,*], Ali Nazari[3], Mohammad Mirjalili[4]

[1] Clothing and Fabric Design Department, Art Faculty, Imam Javad University College, Yazd, Iran
[2] Department of Textile Engineering, Yazd Branch, Islamic Azad University, Yazd, Iran
[3] Department of Art and Architectural,Yazd Branch, Islamic Azad University, Yazd, Iran
[4] Department of Textile Engineering, Yazd Branch, Islamic Azad University, Yazd, Iran

Corresponding Author Email: abghariramin@iauyazd.ac.ir

https://doi.org/10.14447/jnmes.v28i1.a01

Received: June 8-2024

Accepted : December 18-2024

Keywords:
VSM, mechanical properties, saturation magnetic, structural equation, in-situ

ABSTRACT

In this study, silica/Kaolinite/silver nanocomposites were synthesized according to experimental design results, using the central composite design (CCD) method. Samples were synthesized by impregnation on the polyester fabric, to get an in-situ approach to make a new performance of the polyester fabric to protect the human body from dangerous magnetic waves. Initially, magnetic saturation of the designed specimens was tested and its optimum values were measured with a Vibrating Sample Magnetometer (VSM) device. Mechanical properties including tensile strength, friction, abrasion, hydrophobicity (drop absorption), bending, thickness, and Crease Recovery Angle (CRA) of polyester fabrics impregnated with different amounts of nano-composite components were investigated using Response Surface Methodology (RSM) and PLS statistical methods which can help to show the effect of variables on each other. FESEM, EDX, and FTIR analyses were conducted for raw polyester-impregnated nanocomposites using an in-situ method under optimum conditions. The results confirm that the polyester fabric impregnated with three-component nanocomposite by varying concentrations of silica, Kaolinite, and silver, can significantly enhance the properties of saturation magnetic, strength, abrasion, friction, hydrophobicity, bending, thickness, air permeability, and CRA.

1. INTRODUCTION

Textile industry is one of the research areas where nanotechnology can make possible great advances [1-3]. Nanotechnology is based on the fact that properties of the materials will significantly improve when the particle size is reduced to nanometer dimensions [4-6]. A wide range of beneficial properties is obtained in various fields of textile industry [7-8] when nanotechnology and its techniques were used, because it can change the properties of too many materials [9]. Nanomaterials in the range of 100 nm are widely used for industrial applications [10-13]. In this regard, nanotechnology is used effectively to enhance such desirable properties as fabric softness [14-15], durability [16], strength [17], moisture absorption [18], anti-fire [19], and anti-bacterial [20], in fibers, yarns and fabrics [21-23].

Magnetic forces are generated by the motion of charged electrical particles [24-27]. Magnetic field is not a central filed, in other words, there is no one magnetic pole [28-30]. Electrical current in a circular loop of wire creates a magnetic field at the center [31-33]. Therefore, electrons mainly affect magnetic properties of solids [34]. The electrons have a magnetic moment of about 10× 3.9 e.m.u to 21 × 3.9 e.m.u. One of them is magnetic properties of composite materials such as nanocomposites [35], polymers [36], and man-made fibers [37], which a non-conductive particle is added to a metal or polymer matrix in order to modify the magnetic properties [38]. Materials exhibit a variety of magnetic behaviors [39] when they exposed to a magnetic field. According to this, they are classified into some categorizes like diamagnetic [40-44], paramagnetic [45-47], and ferromagnetic [48-51]. However, in some of research papers antiferromagnetic [52-53] and free magnetics are considered as subgroups of ferromagnetic materials [54-58].

Data processing analysis is a multi-step procedure which can obtain data from statistical population, where they (sample) are summarized [59-60], coded [61], categorized and finally processed for applying in various analytical systems to reach a hypothesis testing [62-63]. Data analysis is a process based on science which can apply for any scientific research [64. Therefore, all research activities are controlled and managed until the results to be achieved [65-67]. For this purpose, proposed and designed model is validated using structural equation modeling method [68-71], in order to validate the contained value of each indicator at the measuring desire properties. A comprehensive structural equation model is consisting of path diagram and confirmatory factor analysis. This method widely used in research studies aimed to test a particular model or design a model to get relationship between variables [72-74].

Least squares method does not require a default distribution type for measurement variables [75-77]. If

measurement variables are perceptual, as defined on Likert scale [78], they have an undetermined distribution [79]; therefore, they are abnormal and the least squares method is superior to covariance-oriented methods [80-82]. Covariance- oriented methods are susceptible to sample size [83]. Smaller sample sizes may reduce statistical power of the method [84]. Moreover, with reducing sample size, data normalization assumption will not be displayed greatly [85]. The least squares method can estimate parameters of proposed model using the original sample [86]. However, to achieve a correct statistical estimation of the model [86], it can use re-sampling method to compute confidence intervals for model parameters [87]. Resampling method (e.g. Bootstrapping) validate models using random subsets of the data [88-91]. When parametric clauses (e.g. normality) are not satisfied [92], resampling is another powerful method for statistical inference [93]. Accordingly, least squares method is a powerful and suitable tool when we have some abnormal data and small sample sizes.

Harmful levels of electromagnetic radiation along with new technologies can affect the life quality of people around the world. There is some research about fabricating special goods to protect the human bodies from harmful electromagnetic waves and checking the mechanical and comfortable of the fabrics [113-114] but there has been no comprehensive research on partial least squares statistical analysis on them. This software is not commonly used at textile industries. In this research, a new kind of fabric were synthesized using in situ method to protect people from all harmful electromagnetic waves. Some of experiments such as comfort and mechanical test has been done to confirm as-prepared fabric can consume in the apparel. DX software help us to design the experiments, also Smart PLS software were used to produce as-prepared fabric in industrial size and its real effect on the variables.

1.1. Instrumentation

1.1.1. Materials

Kaolinite Nano clay particles (commercially named as Sillitin N85) were purchased from Haffman Co. (Muenchene Strasse 75 • DE-86633 Neuburg (Donau), Germany). Density of particles was about 2.6 g/cm^3. $AgNO^3$, citric acid (CA) cetyl-trimethyl-ammonium bromide (CTAB) `and Sodium Hypophosphite (SHP) were purchased from Merck Co (8064293, Darmstadt, Germany). The polyester fabrics (with weft and warp densities of 22.1 and 15 yarn/cm and yarn Numerical 150 denier were purchased from yazdbaf Co (Yazd, Iran).

1.1.2. Instruments

Briefly, an Osram UV 400 lamp (HTC 400-241 400W R7S UV LAMP) was used to cure the fabrics with nanocomposites. Surface morphology of the fibers was examined through field emission scanning electron microscopy Via a MIRA3-TESCAN-XMU FE-SEM equipped with a Pulse or Maxim/Quartz Imaging XOne EDX system. Images and EDX analyses were taken using a 15 kV electron accelerating voltage. The presence of Ag, kaolinite and silica particles in the nanocomposites and polyester fabrics was confirmed by EDX system and mapping (Bruker Xflash6/10) which explained above. Tensor 27 (Bruker Germany) infrared spectroscope was applied to evaluate and check the presence of functional group in the impregnated samples.

1.1.3. Method

Design of experiments (DOE)

A design expert toolbox with engineering design tools (related to the response surface methodology) were applied to optimize preparation conditions of polyester fabrics. In our analysis, three independent variables were considered, including Silitin N85 concentration (3.0-9.0 g), $AgNO^3$ (30-60 mL) concentration, and UV irradiation time (30-60 min) (see, Table 1). The effects of these variables on saturated magnetic, strength, abrasion, friction, thickness, bending, crease recovery angle, air permeability and hydrophobic features of the polyester fabrics were evaluated, respectively.

Partial least squares (PLS)

The effect of parameters such as Saturate magnetic, strength, abrasion, friction, hydrophobicity (Drop absorption), bending, thickness, air permeability and CRA in polyester fabrics were investigated using Smart PLS-SEM software to achieve structure modeling.

Table 1. Design of experiments

Run	Sil	silitin N85	UV	Ms	Warp strength(N)	Weft strength(N)	Abrasion	Fri	Drop Absorption	Thickness	Air permeability	Be	Crease
contr	0	0.00	0	0.128	310.8	310.0	986	0.22	20	0.34	60.5	2.1	42
1	45	6.00	45	0.389	318.5	318.2	1145	0.27	152	0.35	41.3	3.85	53
2	45	6.00	45	0.376	322.4	321.5	1144	0.26	150	0.36	38.1	3.56	53
3	45	6.00	19.7	0.305	334.1	333.0	1136	0.22	141	0.4	45.6	4.3	50
4	60	3.00	30	0.313	326.4	325.7	1130	0.26	145	0.33	39.7	3.3	50
5	30	9.00	30	0.397	329.4	328.9	1149	0.23	82	0.36	36.4	3.9	52
6	45	0.95	45	0.259	325.6	324.2	1040	0.30	160	0.37	41.8	3.3	50
7	45	6.00	45	0.353	325.4	324.1	1147	0.27	188	0.36	31.6	3.9	54
8	45	6.00	45	0.391	324.1	323.0	1146	0.28	186	0.35	38.3	3.7	53
9	45	6.00	45	0.379	322.7	321.4	1146	0.27	178	0.35	39.3	3.5	57
10	60	9.00	30	0.426	334.9	333.5	1256	0.23	74	0.36	39.4	3.3	59
11	19.7	6.00	45	0.279	324.8	323.5	1050	0.26	128	0.36	19.6	2.96	51
12	60	9.00	60	0.412	323.6	322.4	1200	0.24	69	0.35	43.2	2.87	58
13	30	9.00	60	0.375	321.4	320.4	1137	0.23	73	0.36	39.4	2.8	57
14	30	3.00	30	0.295	326.8	325.7	1130	0.23	148	0.36	47.2	2.64	54
15	30	3.00	60	0.285	325.6	324.1	1132	0.25	146	0.36	45.2	2.86	55
16	70.2	6.00	45	0.396	329.6	328.5	1211	0.22	188	0.33	51.3	3.14	58
17	45	11.0	45	0.414	333.7	332.6	1136	0.21	171	0.35	35.7	3.58	52
18	45	6.00	70.2	0.321	310.7	309.1	1129	0.25	46	0.35	39.6	3.62	58
19	60	3.00	60	0.312	321.7	320.6	1138	0.26	160	0.34	41.3	2.96	56
20	45	6.00	45	0.388	319.6	318.5	986	0.27	151	0.35	37.2	3.57	53

1.1.4. Preparation of silica/kaolinite/silver nanocomposites and in situ impregnation of polyester

Polyester fabric was prepared with different amounts of Silitin, containing SiO2-kaolinite, as shown in Table 1. Next, different values of an $AgNO^3$ (0.4 N) solution and CTAB (2:1, CTAB/nanocomposite) were added to the mixture and then stirred slowly for 60 minutes. In another side, 8.0% On Weight of fiber (O.W.F) CA and 5.0% (O.W.F) SHP were added to the suspended mixture which was placed in an ultrasound bath for 120 minutes at 50 ºC. The polyester samples immersed in as prepared suspended mixture for 120 seconds and then padded with 85% wet peak up using heavy duty padding mangle (Rapid, Turkey). The samples were dried for four minutes at 60ºC and then cured at room temperature under a 400-W UV irradiation as shown in Table 1. The irradiated fabrics were rinsed with deionized water for three times until the additional and unfixed nanocomposites, CA and SHP were removed. Finally, the treated fabrics were dried in a vacuum drying oven for 1hr at 40ºC.

2. RESULTS AND DISCUSSION

Design of Experiments (DOE)

When a ferromagnetic substance is placed inside a very strong external magnetic field, large amounts of atomic magnetic dipoles will become aligned, along with the external field. Therefore, the volume of alignment along the external field reaches its maximum values. This condition is named magnetic saturation [94].

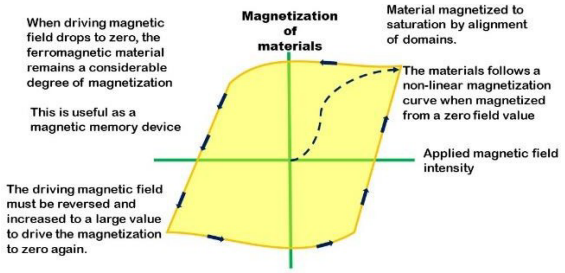

Figure 1. Magnetization of materials

In the present study, the maximum and minimum values of the magnetic saturations were observed in Runs 10 and 11, respectively. This phenomenon indicates that addition of silitin (kaolinite/silica) up to 9 grams to nanocomposite can increase magnetic saturation. In addition, magnetic saturation of Run16 and 11, which contain 70.23 and 19.77 ml of silver nitrate, increase with increasing in silver content. From the above results, it can be concluded that silver can increase magnetic saturation. From the experimental results, it is found that exposure to UV light (254 nm) for more than 45 minutes increases magnetic saturation. The experimental results show that exposure to UV Irradiation for less than 45 minutes can reduce it (see, Run 9 and 18).

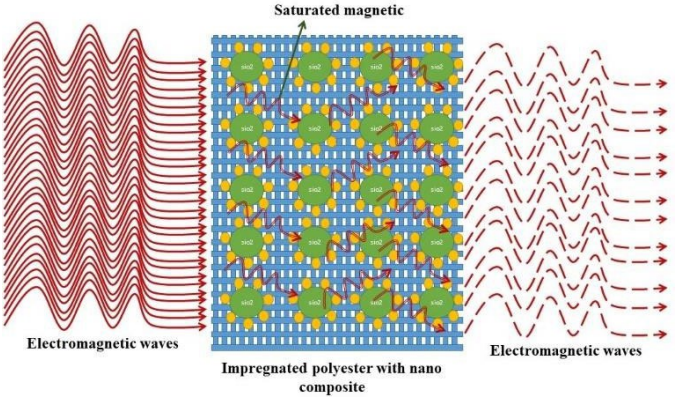

Figure 2. Schematic of saturated magnetic on impregnated polyester fabric with nano composite

Passage of air through the fabric is one of the most important parameters to make clothes more comfortable [96- 98]. Air permeability describes with a standard and must be taken into consideration by the manufacturer which is directly, depends on the fabric usage, according to the ASTM D737 standard, 10 × 10 cm pieces of the fabric specimens were placed between the jaws clamps of the device (METEFEM, Hungry) and then turned it on. For the experiments, we used 4 different air columns. According to the standard method, the largest one relates to the maximum volumetric air flow, and the other columns show air flow rates with higher accuracy. In another hand, sum of numbers which resulted from the columns is used to accurate calculation of absolute air flow rate. Air pressure was adjusted at 100 Pa. This value can vary for different specimens, but it is very important that pressure should be fixed at 100 Pa for different experiments.

From the experimental results, maximum and minimum values of air permeability belonged to Runs 16 and Run11, respectively. The results also reveal that air permeability of the fabric increases with increasing the silver nitrate content. It means that, as prepared samples are more comfortable. Therefore, in-situ coating can reduce air permeability of the polyester fabric.

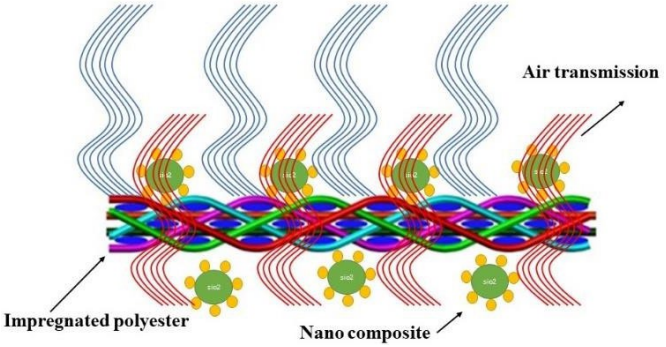

Figure 3. Schematic of air permeability on impregnated polyester with nano composite

Fabric strength tests were conducted to determine the sample resistance along with possible tensions during manufacturing process [99-100]. Strength of fabric is evaluated along the warp or weft directions [101]. Fabrics with different chains, twill and circular warp textures, have an acceptable strength [102]. Fabric strength can be increased by adding some kind of chemical composites to the fabric. According to ASTM D5034 standard,

5.19 × 5 cm pieces of the fabric specimens were placed between the two clamps of the device (MESDAN, Italy) And then their strengths were tested, successfully. In this research, maximum strength value along the warp or weft directions was observed in Run3, where UV irradiation was adjusted at the minimum value. Therefore, change in UV radiation can have a significant effect on

the strength of specimens (see, Run18). A slightly smaller difference was observed between warp and weft directional strengths which is due to the variety in densities of the warp and weft yarns (15.1 and 22.1 cm, respectively).

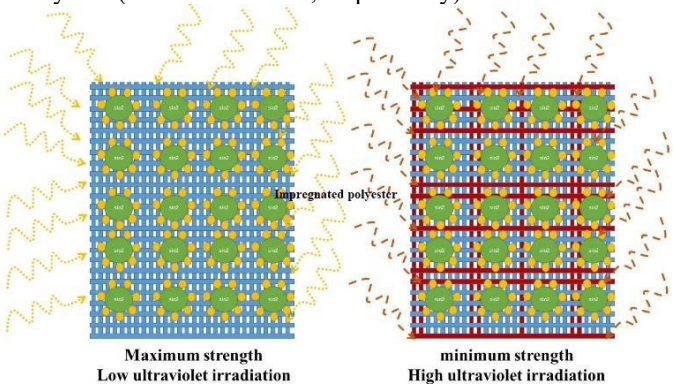

Figure 4. Schematic of strength on impregnated polyester with nano composite, (a) maximum strength by using low ultraviolet irradiation time (b) minimum strength by using high ultraviolet irradiation time

Abrasion resistance test is one of the most important experiments in the textile industry [103]. According to ASTM D3885 (standard test method), 10×10 cm pieces of fabric specimens (regarding to the clamps and their holding sizes) were put into the holding clamps and then the number of cycles which fabric can endure before the yarn breaks was recorded for each specimen. In this experiment, thick texture (new chemical substances coating) increase abrasion resistance of the fabric. In this study, abrasion resistance increased along with the increase in silitin content of three-component nanocomposite. In addition, abrasion resistance decreased along with increasing in ultraviolet irradiation (Run3 and 18).

According to ASTM D3108 standard, 10 × 8 cm pieces of fabric specimens (regarding to metal clamp sizes range) were put into the holding clamps and then plate metal smooth started to move. When the plate was slipping down on the fabric, sensor activated and showed the friction angle. The coefficient of friction (COF) was calculated by the following relation: $\tan\theta=\mu s$ (1)(Where θ is the bend angle of the plate and μs) .

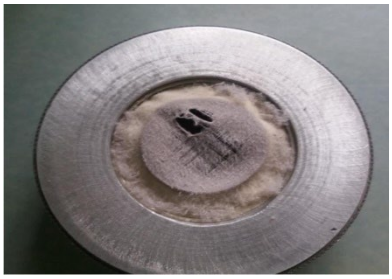

Figure 5. Schematic of abrasion on impregnated polyester with nano composite, (a) High abrasion resistance of the impregnated polyester fabric with nano composite (b) Very low abrasion resistance of the raw polyester fabric

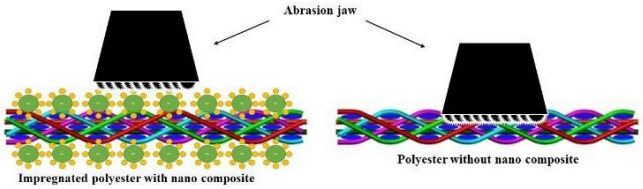

Figure 6. Abrasion test with laboratory machine

As shown in table 1 for run17, friction is smaller than one which observed for the control specimen. It can be concluded that friction decreased by increasing in silitin content of the in- situ impregnated polyester fabric. It can be found that friction decreases along with increasing UV light exposure over 60 minutes, when comparing two experimental results concerning run9 and 18.

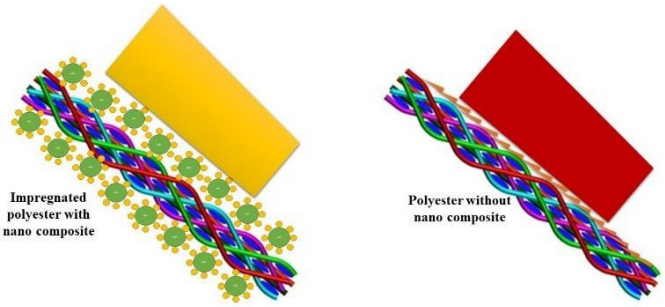

Figure 7. Schematic of friction on impregnated polyester with nano composite, (a) low friction resistance of the impregnated polyester fabric with high ultraviolet irradiation (b) high friction resistance of the raw polyester fabric

According to AATCC 79-2000 standard method, 2.5 × 8 cm pieces of fabric specimens were placed on a glass plate and then a drop of water was poured over them where we used dropper at a 60 ° angle. After that, water absorption of the specimens was measured by a stopwatch. Control specimen test showed a minimum hydrophobicity about 20 seconds. Therefore, in-situ coating of polyester fabrics with silica/Kaolinite/silver can increases hydrophobicity. Experimental results show a maximum hydrophobicity, which is related to run16 and 7, and also a minimum hydrophobicity which is reported for run18. Therefore, hydrophobicity increases with increasing silver nitrate content, and decreases along with increasing ultraviolet light irradiation for more than 45 minutes.

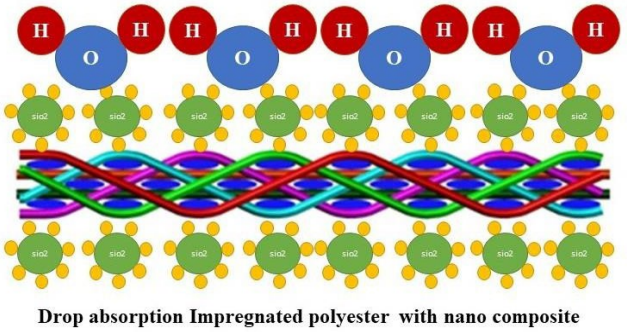

Figure 8. Schematic of drop absorption on impregnated polyester with nano composite

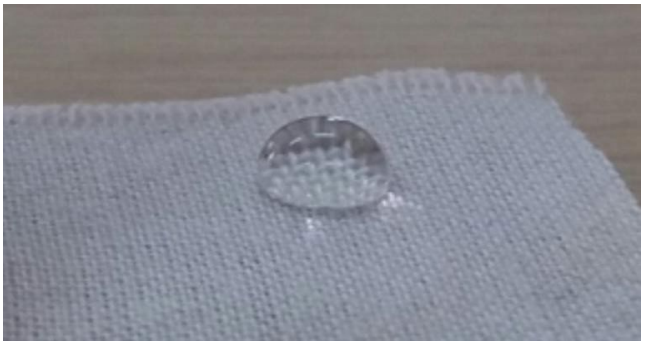

Figure 9. Drop Absorption test

According to ASTM D1777 standard test, 4 × 4 cm pieces of fabric specimens were placed between the clamps of the device and pressure was set as 1 N. In this experiment, thickness display in millimeters when you press the start button. When ultraviolet radiation is minimum, fluffs and staples remain on the fabric surface and they are not destroyed. Hence, thickness reaches its maximum value. Maximum ultraviolet radiation reduces fabric thickness (Run16).

According to ASTM D6828 standard Test, 2.5 × 8 cm pieces of fabric specimens were placed on bending platform with a specific steel ruler on it. Notice that, when the bending reaches the red line, its value is recorded in centimeters.

According to ASTM D3990 standard test, 2.5 × 5 cm pieces of fabric specimens were placed under the weight machines. After 5 minutes, the specimens were placed on a goniometer. First, the crease angle was recorded, and then after 5 minutes, the crease recovery angle was measured which can generate by the following expression:

Crease recovery angle = (Ultimate crease recovery angle) – (Calculated Crease angle).

Statistical analysis

Design Expert is powerful software which is widely used for design of experiments. In the present study, response surface quality optimization tool (RSM)[1] was considered which is widely used for optimizing manufacturing processes and product designs following equations (1 to 10) show the generated mathematical models. Response surface methodology is an optimization methodology which can yield 3D models to show what variable has minimum or maximum effect on the results to solve the problem of researches. This will happen by using a set of mathematical and statistical techniques.

$Ms_{(emu/gr)}$ = +0.38+0.035 × [silver nitrate]+0.046 × [silitin N85]+4.989E-003 × [UV irradiation time]+2.747E-003 × [silver nitrate] × [silitin N85]+2.020E-003 × [silver nitrate] × [UV irradiation time]-3.098E-003 × [silitin N85] × [UV irradiation time]-9.420E-003 × [silver nitrate]^2-9.570E-003 × [silitin N85]^2-0.018 × [UV irradiation time]^2-2.400E-004 × [silver nitrate] × [silitin N85] × [UV irradiation time]+4.361E- 003 × [silver nitrate]^2 × [silitin N85]-0.011 × [silver nitrate]2 × [UV irradiation time]-0.021 × [silver nitrate] × [silitin N85]2 (1)

Strength (Warp) (N) = +313.45+1.84 ×[silver nitrate]+0.34 × [silitin N85]-5.89 × [UV irradiation time]-0.99 ×[silver nitrate]× [silitin N85]-2.11 ×[silver nitrate]× [UV irradiation time]-0.044×[silitin N85]× [UV irradiation time]+1.90 ×[silver nitrate]2+2.66 ×[silitin N85]2+0.42 ×[UV irradiation time]2 (2)

Strength (weft) (N) = +313.68+1.86 ×[silver nitrate]+0.36 ×[silitin N85]-5.98 ×[UV irradiation time]-0.91 ×[silver nitrate]×[silitin N85]-2.11×[silver nitrate]×[UV irradiation time]+0.024 ×[silitin N85]×[UV irradiation time]+1.92 ×[silver nitrate]2+2.60 ×[silitin N85]2+0.48 ×[UV irradiation time]2 (3)

Abrasion (round) =+1142.09+32.71 × [silver nitrate]+27.35 × [silitin N85]-5.11 × [UV irradiation time]+20.50 × [silver nitrate] × [silitin N85]-4.75 × A× [UV irradiation time]-9.75× [silitin N85] × [UV irradiation time]+4.61 × [silver nitrate]2-10.42 × [silitin N85]2+5.31 × [UV irradiation time]2 (4)

Friction (μs) =+0.27-1.072E-003 ×[silver nitrate] -0.017× [silitin N85]+5.838E-003× [UV irradiation time]-1.000E-003× [silver nitrate] × [silitin N85]-5.000E-004 × [silver nitrate] × [UV irradiation time]-2.500E-003× [silitin N85] × [UV irradiation time]-9.257E-003× [silver nitrate]^2-5.898E-003× [silitin N85]^2-0.012× [UV irradiation time]^2 (5)

Drop absorption$_{(s)}$ =+168.31+17.84×+3.27 × [silitin N85]-

Air permeability $_{(m^3/m^2/1hr/100pa)}$ =+37.58+9.45 × [silver nitrate] -1.80 × [silitin N85]-1.77 × [UV irradiation time]+2.28 × silver nitrate] × silitin N85]+0.55 × silver nitrate] × UV irradiation time]+0.89 × silitin N85] × [UV irradiation time]-0.25 × silver nitrate] ^{2}+0.91 × silitin N85]^2+2.28 × UV irradiation time]^2-0.35× silver nitrate] × silitin N85] × [UV irradiation time]-0.078× silver nitrate] ^{2} × silitin N85]+2.59 × silver nitrate] ^{2}× UV irradiation time]-10.02 × silver nitrate] × silitin N85]^2 (8)

Bending $_{(cm)}$ = +3.69 +0.039 ×[silver nitrate]+0.12 × [silitin N85]-0.20 × [UV irradiation time]-0.16 × [silver nitrate] × [silitin N85]+0.014× [silver nitrate] × [UV irradiation time]-0.18× [silitin N85] × [UV irradiation time]-0.31× [silver nitrate]^2-0.17 × [silitin N85]^2+0.016 × [UV irradiation time]^2 (9)

Crease Recovery Angle $_{(CRA)}$ = +54.15+1.23 × [silver nitrate]+1.05 × [silitin N85]+1.79 × [UV irradiation time] (10)

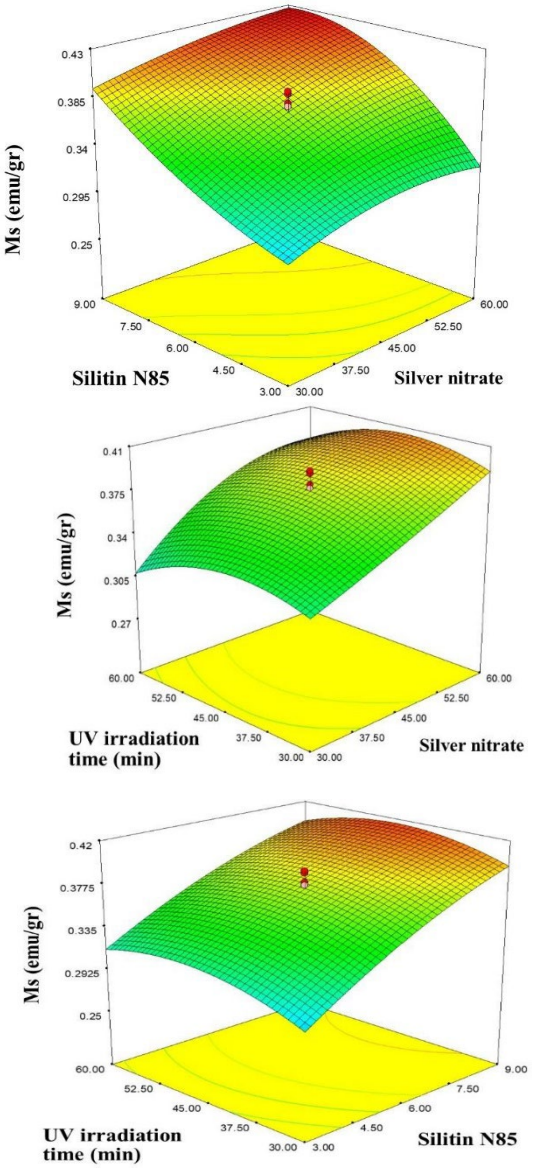

Figure 10. Response surface for Ms (emu/gr) as a function of: (a) $AgNO_3$ and silitin N85, (b) $AgNO_3$ and UV irradiation time, (c) UV irradiation time and silitin N85

According to the figure (10), there is a response for the Ms (emu/gr) in three 3D charts. Chart (a) can show that silver nitrate in 60 ml with 52.50 min UV irradiation time is the best situation for high Ms(emu/gr). In chart (b) which is showing silitin N85 and

silver nitrate effect, the high red peak in chart is for 9 gr and 60 ml of the materials. The last chart (c) showing the effect of silitin N85 and UV Irradiation time which has high peak in red color for 45 min and 9 gr.

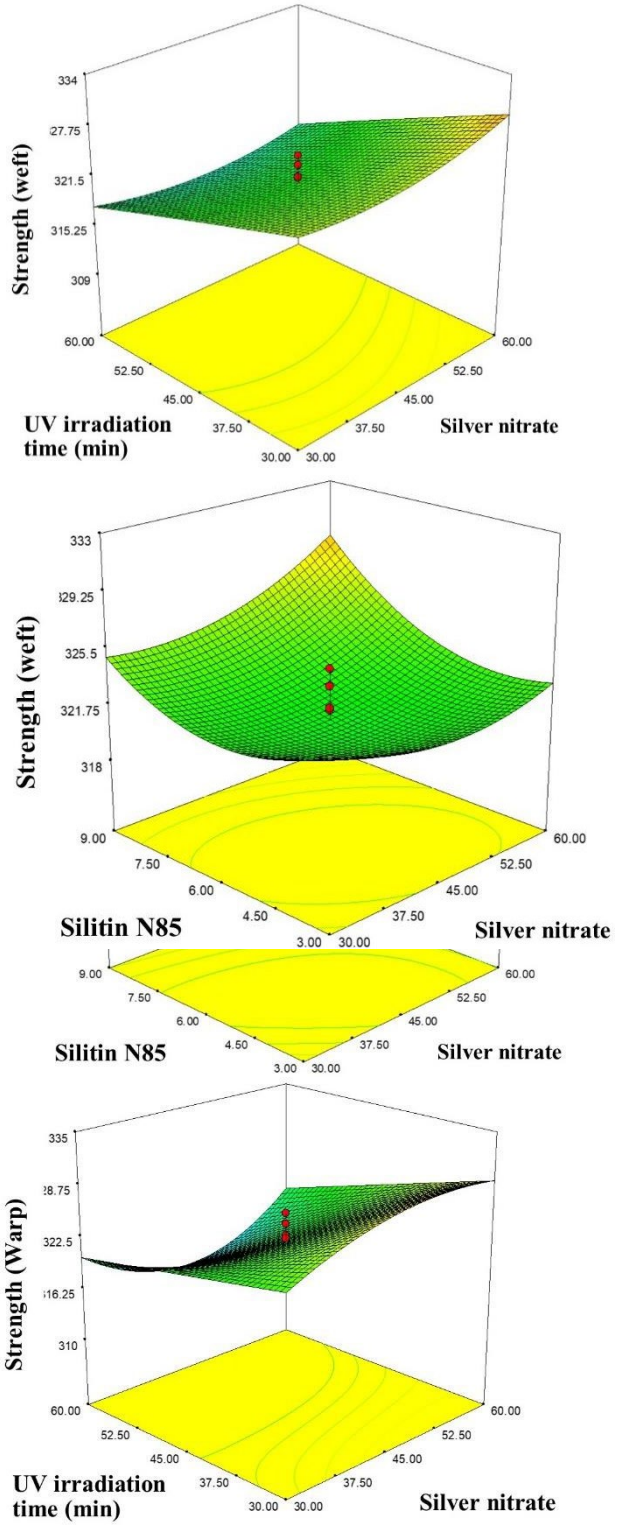

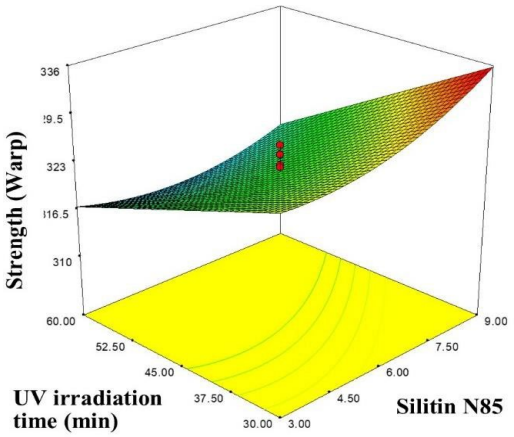

Figure 11. Response surface for strength(warp) as a function of: (a) $AgNO_3$ and silitin N85, (b) $AgNO_3$ and UV irradiation time, (c) UV irradiation time and silitin N85

According to the Figure (11), here the warp strength of fabric tested which is showing that in chart (a), silver nitrate has good effect by 60 ml and silitin N85 can improve these properties with 9 gr value. In Chart (b) there is a high peak at the right of the chart with green and yellow color which is the best result for the strength. Chart (c), strength has significant effect from UV and silitin N85 which is showing by red color.

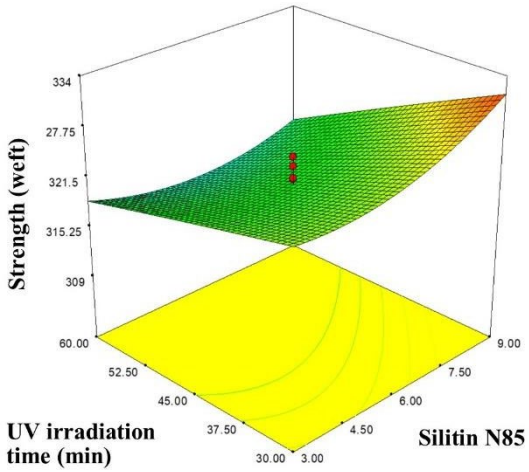

Figure 12. Response surface for strength(weft) as a function of: (a) $AgNO_3$ and silitin N85, (b) $AgNO_3$ and UV irradiation time, (c) UV irradiation time and silitin N85

Weft strength has same result like the warp strength which is showing that the composite has same effect on fabric structure. The highest effect is for Silitin N85 and UV irradiation.

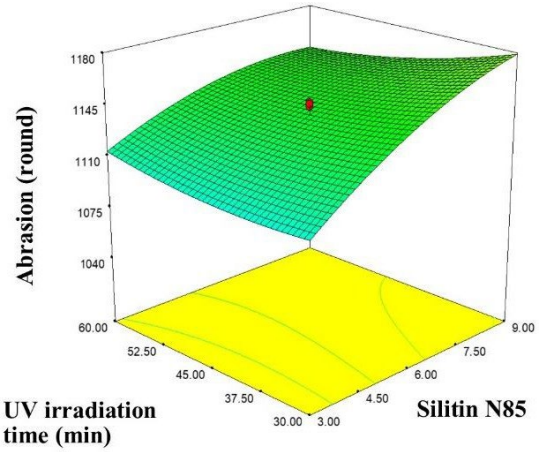

Figure 13. Response surface for Abrasion (round) as a function of: (a) $AgNO_3$ and silitin N85, (b) $AgNO_3$ and UV irradiation time, (c) UV irradiation time and silitin N85

According to the figure (13), 3D chart (a) is showing the effect of the Silitin N85 and silver nitrate for the fabric abrasion. The best fabric abrasion is 1220 round which is showing by the yellow color on the chart. In chart (b), the optimization of the abrasion by the 30 min UV irradiation and 60 ml silver nitrate is 1117 round. The best result for the silitin N85 and UV irradiation can see in chart (c) which is 1145 round.

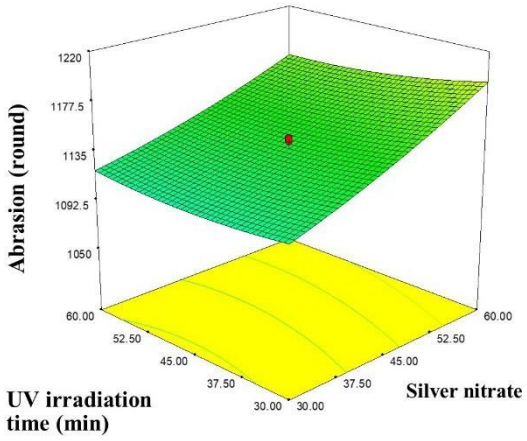

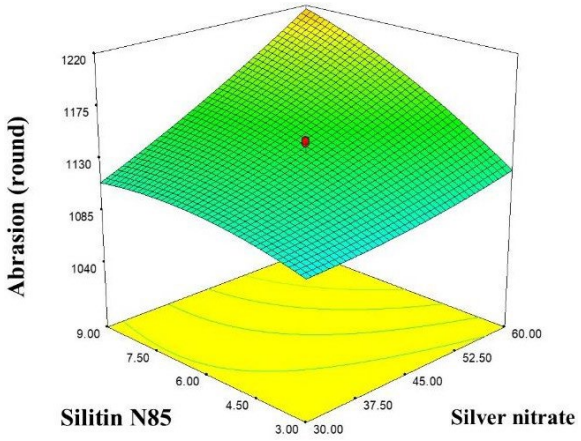

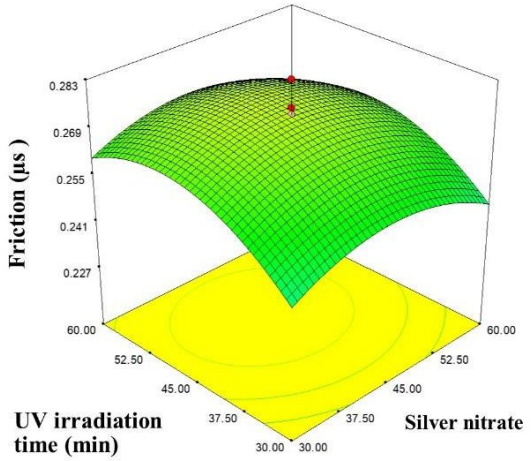

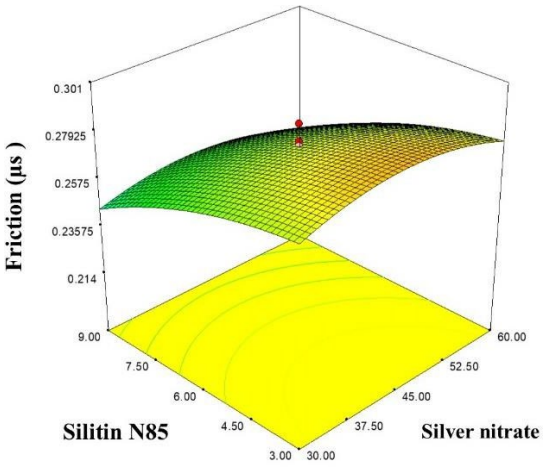

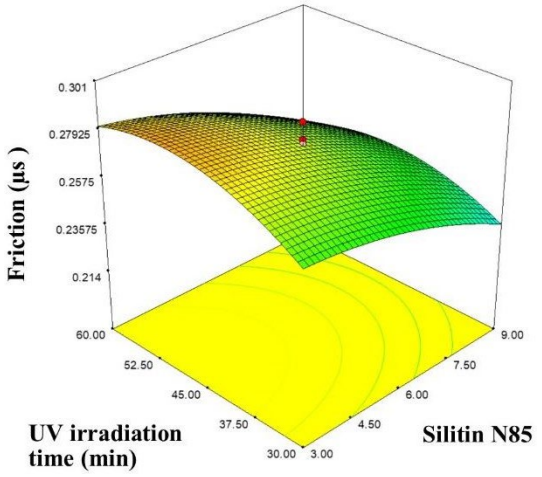

Figure 14. Response surface for Friction (µs) as a function of: (a) $AgNO_3$ and silitin N85, (b) $AgNO_3$ and UV irradiation time, (c) UV irradiation time and silitin N85

According to the figure (14), there is a normal behavior of the material. In chart (a), the yellow color of the chart can show the trend of the friction behavior because of the materials. The highest peak is for the 38 ml silver nitrate and 3.5 gr Silitin N85. Chart (b), 45 ml silver nitrate and 45 min UV irradiation is the best result for the friction of the fabric.

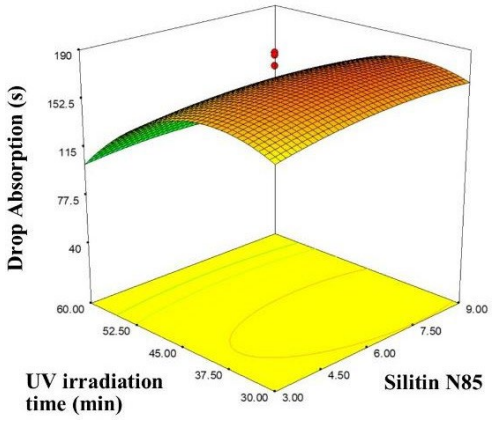

Figure 15. Response surface for Drop Absorption (s) as a function of: (a) $AgNO_3$ and silitin N85, (b) $AgNO_3$ and UV irradiation time, (c) UV irradiation time and silitin N85

There is a huge difference in chart (a) about materials behavior in Drop absorbtion test. There is two high peaks in red color, one is for the silver nitrate 30ml / Silitin N85 30gr and another is for silver nitrate 60 ml/Silitin N85 30 gr. It is showing that after increasing silver nitrate up to 60, the optimization of the drop absorption will be increase. Chart (b) is showing that there is dramatically drop absorption time increasing because of the UV irradiation time which colored by red. Chart (c) has smooth growing in uv irradiation time (45min). after that by the increasing the time of irradiation, the drop absorption time is going down.

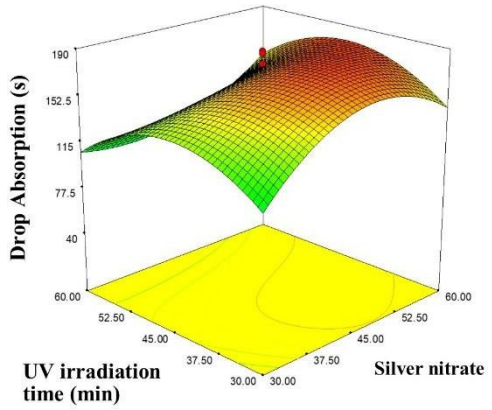

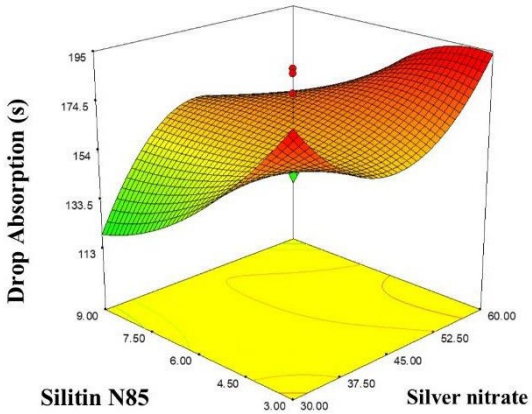

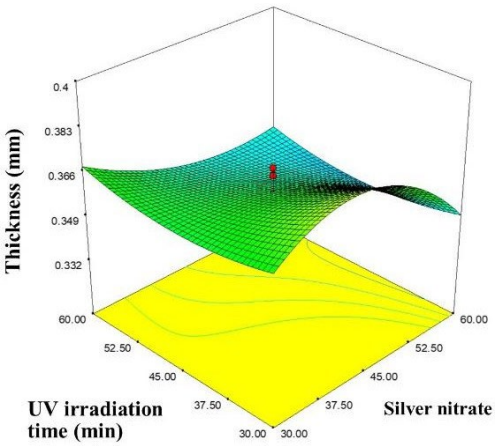

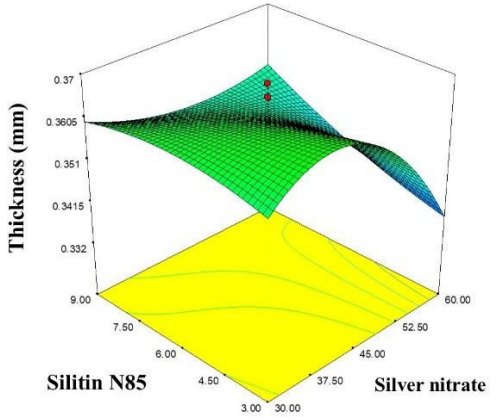

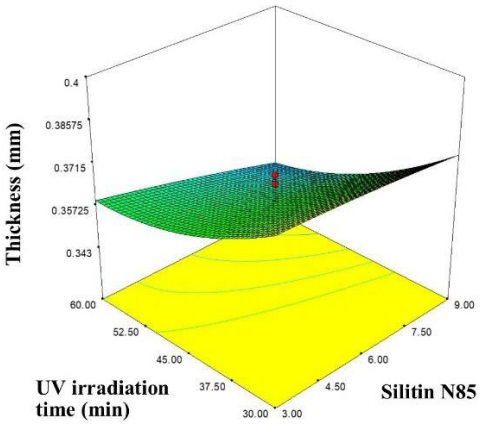

Figure 16. Response surface for Thickness (mm) as a function of: (a) $AgNO_3$ and silitin N85, (b) $AgNO_3$ and UV irradiation time, (c) UV irradiation time and silitin N85

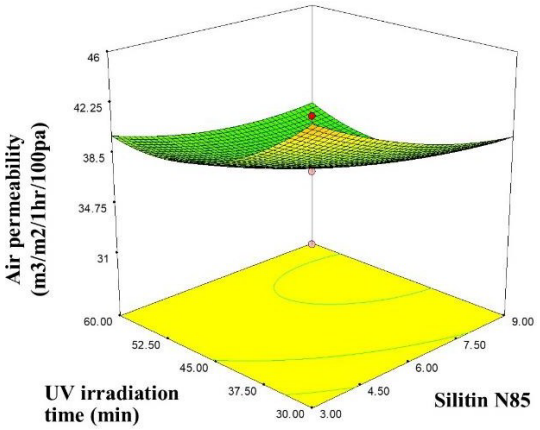

Figure 17. Response surface for Air permeability (m3/m3/1hr/100pa) as a function of: (a) $AgNO_3$ and silitin N85, (b) $AgNO_3$ and UV irradiation time, (c) UV irradiation time and silitin N85

According to the figure (16), the thickness of the fabric has some changes which is showing in all charts. The highest changing in chart (a) happened by increasing Silitin N85 component which is predicable. In chart (b) thickness decreased by the UV irradiation time which is showing that UV Irradiation can destroyed some of the layers on the top or bottom of the fabric. Chart (c) showing that by increasing silitin N85 again the thickness will change.

According to the figure (17), the air permeability is increasing in silver nitrate 65ml and Silitin N85 6 gr (chart (a)), in chart (b), there is twi high peak which is highlighted by the red color in the corner of the shape. When the silver nitrate is 60 ml, in UV irradiation time at the minimum and maximum there is high air permeability. Chart (3), has smoothly changes. The optimize point is in yellow color.

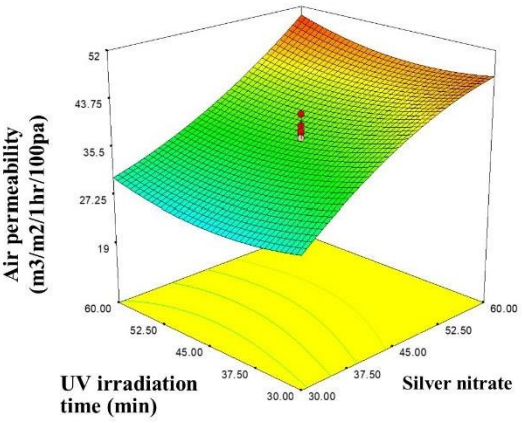

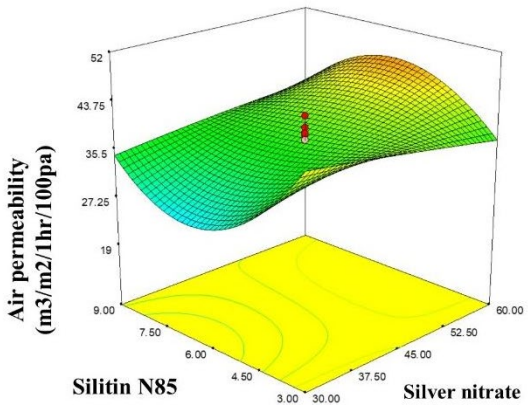

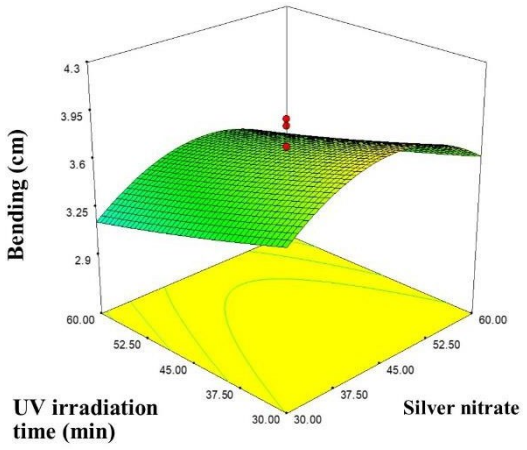

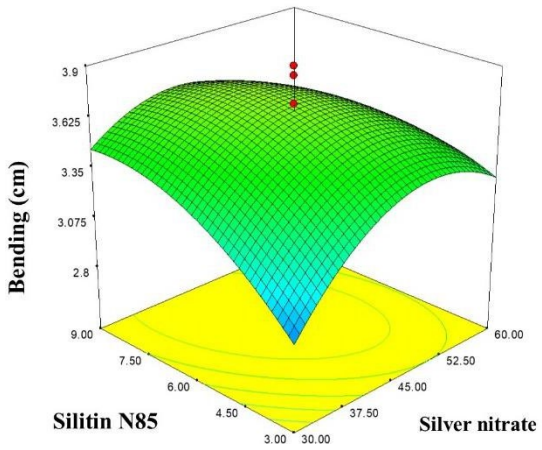

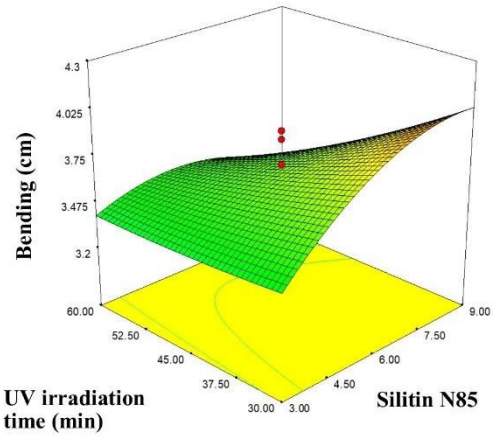

Figure 18. Response surface for Bending (cm) as a function of: (a) $AgNO_3$ and silitin N85, (b) $AgNO_3$ and UV irradiation time, (c) UV irradiation time and silitin N85

Regarding the figure (18), there is the low peak by the blue color which is showing that minimum silver nitrate and Silitin N85 have low affect on fabric bending. Chart (b) is showing that the silver nitrate 45 ml and UV irradiation 45 min can deliver the optimize bending. In Chart (c), low UV irradiation with high silitin N85 component can deliver the optimize bending in fabric.

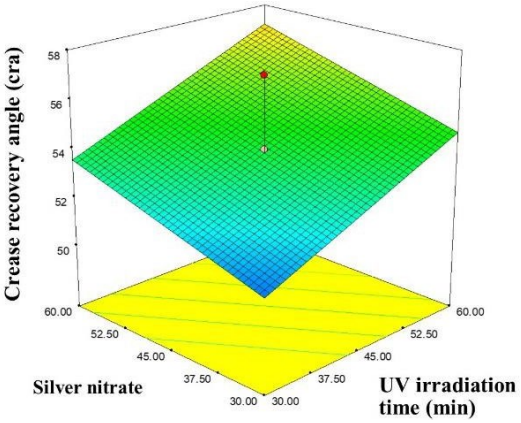

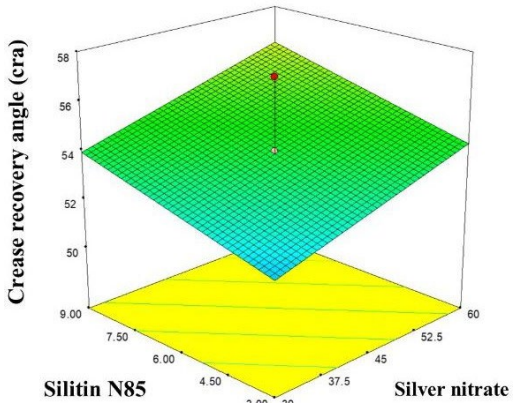

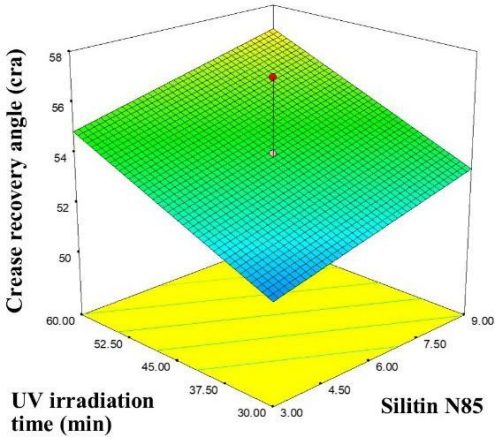

Figure 19. Response surface for crease recovery angle (cra) as a function of: (a) $AgNO_3$ and silitin N85, (b) $AgNO_3$ and UV irradiation time, (c) UV irradiation time and silitin N85

One of the simple models in DX software is linear. Regarding all charts in figure (19), when the nanocomposite components are high the CRA is optimize.

RSM not only can reduce the computational and simulation cost, but also predicts and shows normal trend of process optimization which is mainly followed with non-linear relationships. Although the generated models are second, third, or sometimes fourth order, many optimization and decision making programs cannot generate third- (or higher) order models. In the other words, they are less able to find the optimum ultimate response. ANOVA test was used (Design -Expert software, version 7.0.0.1) to investigate and determine the difference between response surface.

Table 2. ANOVA results of saturated magnetic for polyester impregnated with nanocomposite

ANOVA for Response Surface Cubic Model					
Source	**Sum of Squares**	**Df**	**Mean Square**	**F Value**	**p-value Prob > F**
Model	0.0477273	13	0.0036713	7.0320793	0.0125
A-silver	0.0069384	1	0.0069384	13.289862	0.0108
B-silitin n 85	0.012011	1	0.012011	23.005794	0.0030
C-UV	0.0001408	1	0.0001408	0.2696583	0.0222
AB	6.039E-05	1	6.039E-05	0.1156712	0.7454
AC	3.264E-05	1	3.264E-05	0.0625248	0.8109
BC	7.676E-05	1	7.676E-05	0.1470187	0.7146
A^2	0.0012788	1	0.0012788	2.4494858	0.1686
B^2	0.00132	1	0.00132	2.5282525	0.1629
C^2	0.0046789	1	0.0046789	8.9619292	0.0242
ABC	4.608E-07	1	4.608E-07	0.0008826	0.9773
A^2B	6.303E-05	1	6.303E-05	0.1207218	0.7401
A^2C	0.0004062	1	0.0004062	0.7779746	0.4117
AB^2	0.0014738	1	0.0014738	2.8230131	0.1439
Residual	0.0031325	6	0.0005221		
Lack of Fit	0.0021052	1	0.0021052	10.246877	0.0240
Pure Error	0.0010273	5	0.0002055		
Cor Total	0.0508598	19			

According to table 2, test reliability was smaller than 0.05 for the RSM Proposed model. There is a significant difference between the effects of different variables on magnetic saturation. Hence, it can be concluded that silver nitrite, silitin, and UV radiation can have a significant effect on optimization of magnetic saturation of in-situ impregnated polyester fabric with silica / Kaolinite / silver nanocomposite. Since F-statistic parameter for silitin is higher than the F-statistic of model, silitin content has a greater impact on magnetic saturation.

Figure 20 shows magnetic saturation of the optimized specimen. The maximum magnetic saturation belongs to the optimum specimen (41.5599×10^{-3} emu/g).

Table 3. ANOVA results of air permeability for polyester impregnated with nanocomposite

ANOVA for Response Surface Cubic Model					
Source	**Sum of Squares**	**Df**	**Mean Square**	**F Value**	**p-value**
Model	714.3922	13	54.95324	4.549858	0.0366
A-silver	504.6665	1	504.6665	41.7839	0.0007
B-silitin n 85	18.41031	1	18.41031	1.524283	0.2631
C-UV	17.81448	1	17.81448	1.474951	0.2702
AB	41.74695	1	41.74695	3.456442	0.1124
AC	2.414503	1	2.414503	0.199909	0.6705
BC	6.399253	1	6.399253	0.529827	0.4941
A^2	0.88472	1	0.88472	0.073251	0.7957
B^2	11.89996	1	11.89996	0.985258	0.3592
C^2	74.70396	1	74.70396	6.18512	0.0474
ABC	0.962578	1	0.962578	0.079697	0.7872
A^2B	0.020082	1	0.020082	0.001663	0.9688
A^2C	22.18956	1	22.18956	1.837186	0.2241
AB^2	332.8406	1	332.8406	27.55757	0.0019
Residual	72.46807	6	12.07801		
Lack of Fit	19.00139	1	19.00139	1.776937	0.2400
Pure Error	53.46668	5	10.69334		
Cor Total	786.8602	19			

Table 4. ANOVA results of friction for polyester impregnated with nanocomposite

ANOVA for Response Surface Quadratic Model					
Source	**Sum of Squares**	**Df**	**Mean Square**	**F Value**	**p-value**
Model	0.0074633	9	0.0008293	3.5755005	0.0299
A-silver	1.568E-05	1	1.568E-05	0.0676242	0.8001
B-silitin n 85	0.0037504	1	0.0037504	16.170712	0.0024
C-UV	0.0004654	1	0.0004654	2.0068058	0.1870
AB	8E-06	1	8E-06	0.0344937	0.8564
AC	2E-06	1	2E-06	0.0086234	0.9278
BC	0.00005	1	0.00005	0.2155854	0.6524
A^2	0.001235	1	0.001235	5.3248015	0.0437
B^2	0.0005014	1	0.0005014	2.1617937	0.1722
C^2	0.0019836	1	0.0019836	8.5525459	0.0152
Residual	0.0023193	10	0.0002319		
Lack of Fit	0.0021773	5	0.0004355	15.332861	0.0047
Pure Error	0.000142	5	0.0000284		
Cor Total	0.0097826	19			

Table 5. ANOVA results of drop absorbtion for polyester impregnated with nanocomposite

ANOVA for Response Surface cubic Model					
Source	**Sum of Squares**	**Df**	**Mean Square**	**F Value**	**p-value**
Model	32734.205	13	2518.016	4.071171	0.0474
A-silver	1800	1	1800	2.910271	0.1389
B-silitin n 85	60.5	1	60.5	0.097817	0.7651
C-UV	4512.5	1	4512.5	7.295887	0.0355
AB	66.125	1	66.125	0.106912	0.7548
AC	55.125	1	55.125	0.089127	0.7754
BC	91.125	1	91.125	0.147332	0.7143
A^2	1082.0835	1	1082.084	1.749531	0.2341
B^2	521.15357	1	521.1536	0.84261	0.3941
C^2	14271.835	1	14271.84	23.07495	0.0030
ABC	21.125	1	21.125	0.034155	0.8595
A^2B	5541.9361	1	5541.936	8.960297	0.0242
A^2C	2620.0153	1	2620.015	4.236086	0.0853
AB^2	1069.2449	1	1069.245	1.728774	0.2366
AC^2	32734.205	13	2518.016	4.071171	0.0474
B^2C	1800	1	1800	2.910271	0.1389
BC^2	60.5	1	60.5	0.097817	0.7651
A^3	4512.5	1	4512.5	7.295887	0.0355
B^3	66.125	1	66.125	0.106912	0.7548
C^3	55.125	1	55.125	0.089127	0.7754
Residual	3710.9948	6	618.4991		
Lack of Fit	2019.4948	1	2019.495	5.969538	0.0584
Pure Error	1691.5	5	338.3		
Cor Total	36445.2	19			

Table 6. ANOVA results of abrasion for polyester impregnated with nanocomposite

Source	**Squares**		**Square**	**Value**	
Model	32015.202	9	3557.2447	4.0228731	0.0204
A-silver	14615.534	1	14615.534	16.528647	0.0023
B-silitin n 85	10212.197	1	10212.197	11.54893	0.0068
C-UV	356.46633	1	356.46633	0.4031263	0.5397
AB	3362	1	3362	3.8020717	0.0798
AC	180.5	1	180.5	0.2041267	0.6611
BC	760.5	1	760.5	0.8600463	0.3756
A^2	305.74378	1	305.74378	0.3457644	0.5696
B^2	1564.7208	1	1564.7208	1.7695362	0.2130
C^2	406.8234	1	406.8234	0.4600749	0.5130
Residual	8842.5476	10	884.25476		
Lack of Fit	8705.0476	5	1741.0095	63.309437	0.0002
Pure Error	137.5	5	27.5		
Cor Total	40857.75	19			

Table 7. ANOVA results of strenght(warp) for polyester impregnated with nanocomposite

ANOVA for Response Surface cubic Model					
Source	**Sum of Squares**	**Df**	**Mean Square**	**F Value**	**p-value**
Model	583.16483	13	44.858833	7.6146246	0.0101
A-silver	11.476841	1	11.476841	1.9481522	0.2123
B-silitin n 85	32.9672	1	32.9672	5.5960629	0.0559
C-UV	274.85746	1	274.85746	46.656059	0.0005
AB	18.280081	1	18.280081	3.1029776	0.1286
AC	5.8259911	1	5.8259911	0.9889409	0.3584
BC	22.114575	1	22.114575	3.7538691	0.1008
A^2	41.198215	1	41.198215	6.993248	0.0383
B^2	94.393193	1	94.393193	16.022903	0.0071
C^2	0.000703	1	0.000703	0.0001193	0.9916
ABC	0.0026281	1	0.0026281	0.0004461	0.9838
A^2B	5.7888225	1	5.7888225	0.9826317	0.3598
A^2C	48.036811	1	48.036811	8.1540748	0.0290
AB^2	3.2264627	1	3.2264627	0.5476804	0.4872
Residual	35.34685	6	5.8911417		
Lack of Fit	0.6149691	1	0.6149691	0.0885309	0.7780
Pure Error	34.731881	5	6.9463763		
Cor Total	618.51168	19			

ANOVA for Response Surface cubic Model					
	Sum of	**Df**	**Mean**	**F**	**p-value**

Table 8. ANOVA results of strenght(weft) for polyester impregnated with nanocomposite

ANOVA for Response Surface Quadratic Model					
Source	**Sum of Squares**	**Df**	**Mean Square**	**F Value**	**p-value**
Model	716.79261	9	79.643623	7.0420963	0.0026
A-silver	47.276989	1	47.276989	4.1802356	0.0681
B-silitin n 85	1.7363782	1	1.7363782	0.1535307	0.7034
C-UV	487.78824	1	487.78824	43.13028	< 0.0001
AB	6.6813401	1	6.6813401	0.5907647	0.4599
AC	35.680128	1	35.680128	3.1548401	0.1061
BC	0.0047531	1	0.0047531	0.0004203	0.9840
A^2	53.082025	1	53.082025	4.6935174	0.0555
B^2	97.392048	1	97.392048	8.6114136	0.0149
C^2	3.3042306	1	3.3042306	0.2921604	0.6007
Residual	113.09647	10	11.309647		
Lack of Fit	89.269362	5	17.853872	3.7465464	0.0867
Pure Error	23.827107	5	4.7654214		
Cor Total	829.88908	19			

Table 9. ANOVA results of thickness for polyester impregnated with nanocomposite

ANOVA for Response Surface cubic Model					
Source	**Sum of Squares**	**Df**	**Mean Square**	**F Value**	**p-value**
Model	0.0033048	13	0.0002542	5.166413	0.0270
A-silver	0.0004205	1	0.0004205	8.5458879	0.0265
B-silitin n 85	0.000162	1	0.000162	3.2923516	0.1195
C-UV	0.000968	1	0.000968	19.672817	0.0044
AB	0.0001445	1	0.0001445	2.9366963	0.1374
AC	0	1	0	0	1.0000
BC	6.05E-05	1	6.05E-05	1.2295511	0.3100
A^2	0.0004767	1	0.0004767	9.6885764	0.0208
B^2	5.629E-06	1	5.629E-06	0.1144074	0.7467
C^2	0.000418	1	0.000418	8.4943712	0.0268
ABC	0.000072	1	0.000072	1.4632674	0.2719
A^2B	0.0003216	1	0.0003216	6.5358823	0.0431
A^2C	0.0006339	1	0.0006339	12.883389	0.0115

Table 10. ANOVA results of bending for polyester impregnated with nanocomposite

ANOVA for Response Surface Quadratic Model					
Source	**Sum of Squares**	**Df**	**Mean Square**	**F Value**	**p-value**
Model	2.9046866	9	0.322743	3.8865569	0.0228
A-silver	0.0207803	1	0.0207803	0.2502419	0.6277
B-silitin n 85	0.1830034	1	0.1830034	2.2037762	0.1685
C-UV	0.5714572	1	0.5714572	6.8816404	0.0255
AB	0.2080125	1	0.2080125	2.5049421	0.1446
AC	0.0015125	1	0.0015125	0.0182139	0.8953
BC	0.2485125	1	0.2485125	2.9926539	0.1143
A^2	1.3458722	1	1.3458722	16.207352	0.0024
B^2	0.4053516	1	0.4053516	4.8813527	0.0516
C^2	0.0037521	1	0.0037521	0.0451837	0.8359
Residual	0.8304084	10	0.0830408		
Lack of Fit	0.6938084	5	0.1387617	5.0791245	0.0495
Pure Error	0.1366	5	0.02732		
Cor Total	3.735095	19			

Table 11. ANOVA results of crease recovery angle for polyester impregnated with nanocomposite

ANOVA for Response Surface Quadratic Model					
Source	**Sum of Squares**	**Df**	**Mean Square**	**F Value**	**p-value**
Model	79.49458	3	26.498193	4.9846452	0.0125
A-silver	20.599065	1	20.599065	3.8749446	0.0666
B-silitin n 85	15.10689	1	15.10689	2.841797	0.1112
C-UV	43.788625	1	43.788625	8.2371941	0.0111
Residual	85.05542	16	5.3159637		
Lack of Fit	72.222087	11	6.5656442	2.5580432	0.1550
Pure Error	12.833333	5	2.5666667		
Cor Total	164.55	19			

Table 12. polyester modified with factors affecting at their mechanical and magnetic properties

Solutions	UV min	Siliti N85 (gr)	Silve 0.4 (ml)	MS	Nemu/gr	Strength (N)	Abrasion resistanc (round)	Frictio s)	Drop bsorptio (s)	hickne	Air rmeabili	endin	CRA
MS	5.0	9.00	45.78	1.559E 3	-	-	-	-	-	-	-	-	-
Strength (warp)	0.0	9.00	45.00	-	331.25	-	-	-	-	-	-	-	-
Strength (weft)	0.0	9.00	45.00	-	331.35	-	-	-	-	-	-	-	-
Abrasion resistance	5.0	9.00	40.00	-	-	1220.57	-	-	-	-	-	-	-
Friction	0.0	9.00	45.00	-	-	-	0.2330	-	-	-	-	-	-
Drop absorption	0.0	8.92	53.25	-	-	-	-	141.106	-	-	-	-	-
Thickness	0.0	7.60	60.00	-	-	-	-	-	0.356	-	-	-	-
Air emeabilit	6.7	7.37	60.00	-	-	-	-	-	-	47.727	-	-	-
Bending	0.0	8.98	45.00	-	-	-	-	-	-	-	3.87	-	
CRA	0.0	9.00	45.00	-	-	-	-	-	-	-	-	54.077	

Table 13. properties of VSM output details for testing saturate magnetic in polyester fabric impregnated with in situ nano composite synthesis

Coercivity (Hci)	48.877 G
Initial Slope	16.806E-3 emu/(g G)
Magnetization (Ms)	41.559E-3 emu/g
Mass	34.390E-3 g
Retentivity (Mr)	1.0445E-3emu/g

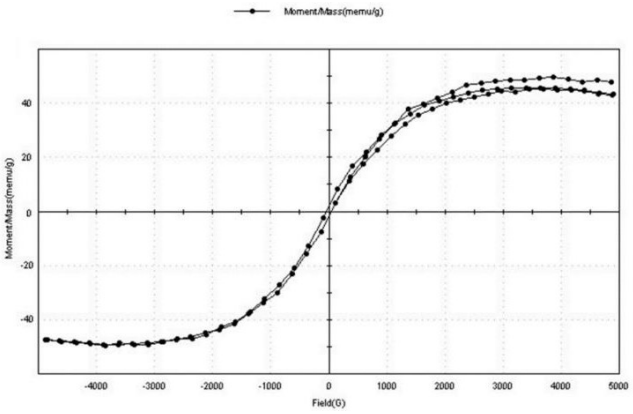

Figure 20. saturate magnetic diagram of polyester fabric impregnated with in situ nano composite synthesis from VSM test (5000 into -5000 G magnetic field)

Referring to Fig. 20 it is observe that optimized polyester specimen is stable along with the magnetic saturation of about 41 (emu/g), where magnetic field is in the range from 3000 G to 4000 G.

Morphology of the polyester

FESEM is one of the best methods to investigate morphology of Kaolinite. Figure 21 shows the results of FESEM analysis of Kaolinite/silica/silver particles on polyester fibers obtained implying in-situ impregnation method with different magnification.

According to the figure21 Kaolinite flakes shows a thin structure with an average diameter of about 29 nm. The particles consist of dense and curved plates which fit well into polyester fibers by the same way. FESEM results reveal that spherical silver nanoparticles were heterogeneously distributed with the size ranging from 66 to 72 nanometers. According to figure 21, the flaky layers of kaolinite particles have a thin structure showing a high aspect ratio. The composite of silver/silica/kaolinite showing different textures of the kaolinite flat surface with aggregated AgNPs. Results indicated that embedded AgNPs possess a nearly coarse spherical morphology with a heterogeneous distribution and influence strongly the final nanocomposite morphology [111].

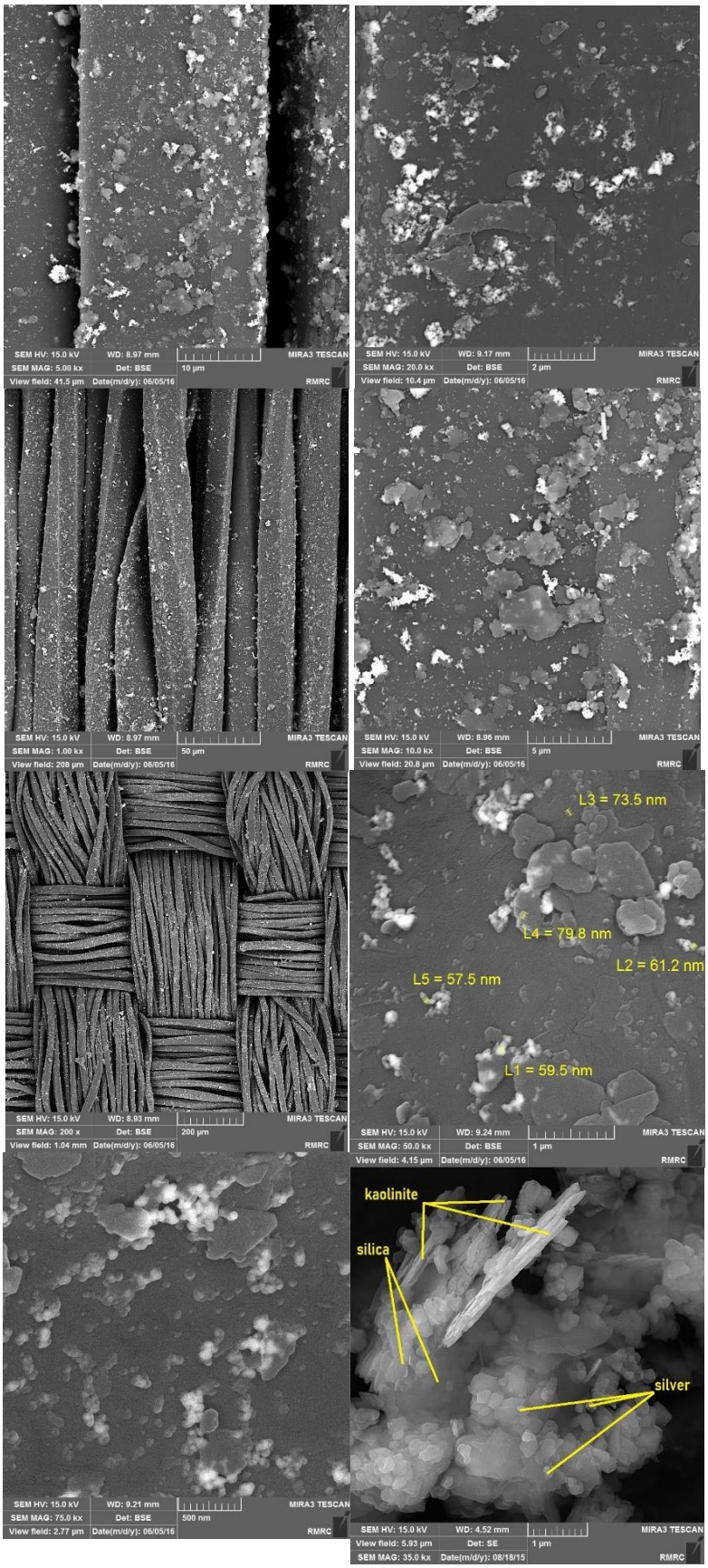

Figure 21. The FESEM images of the impregnated polyester by nanocomposite at the magnification of (a) 200x, (b) 1.00 kx, (c) 5.00 kx. (d) 10.00 kx, (e) 20.00 kx, (f) 75.00 kx (g) 50.00 kx (h) 35.00 kx of silica/kaolinite/silver

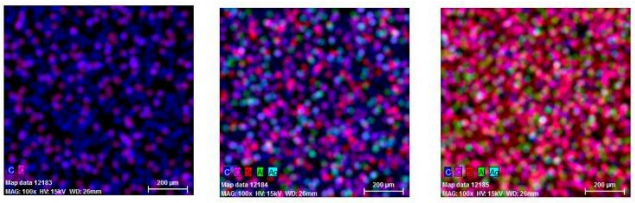

Figure 22. The Mapping/EDX images of raw polyester (a), impregnated polyester fabric by nanocomposite (b), synthetic nanocomposite (c)

This analysis done on the surface of the raw polyester fabric, modified and nanocomposite particles. We have investigated the successful synthesis of nanocomposite and fabric modification. The presence of Si, O, C, Al, and Ag in the synthetic composite is clearly visible, which is in good agreement with the SEM and FTIR analyzes and confirms the successful synthesis and modification (Figure 22-c).
Comparison of (a) and (b) spectra clearly shows that good modification and uniform distribution of nanocomposites on the fabric surface with presence of C and O elements in the raw polyester fabric spectrum and Ag, Si and Al elements in addition to C and O in the modified fabric spectrum.

EDX analysis

EDX is a powerful analysis to study the elemental composition of Kaolinite and Kaolinite/silica/silver compound. Figs. 23 and 24 display the elemental EDX results of the fabricated nanocomposites. The samples were gold sputtered before examination. According to Tables 14 and 15, the characteristic peaks in the spectrum for untreated particles are associated with Al, Si, Mg, Ca, Ti, K, and Fe. Also the EDX results show that silver is added to the Kaolinite/silica nanocomposite after UV exposure. The experimental results reveal that content of different elements in Kaolinite structure is varied by UV light irradiation.

Table 14. EDX analysis in raw polyester fabric

Elt	Line	Int	Error	K	Kr	W%	A%	ZAF	Pk/Bg	LConf	HConf
C	Ka	583.7	25.2989	0.9277	0.5763	74.51	79.56	0.7734	132.71	73.21	75.81
O	Ka	91.3	5.2716	0.0723	0.0449	25.49	20.44	0.1762	65.98	24.37	26.62
				1.0000	0.6212	100.00	100.00				

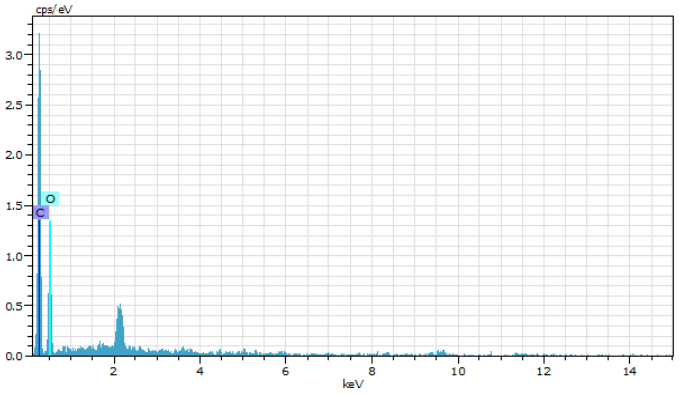

Figure 23. EDX analysis of polyester

Table 15. EDX analysis in polyester modified with in situ nano composite synthesis

Elt	Int	K	Kr	W%	A%	ZAF	Pk/Bg	LConf	HConf
C	235.2	0.6212	0.2766	55.28	69.40	0.5004	146.65	54.21	56.36
O	106.4	0.1400	0.0623	28.61	26.96	0.2179	58.29	27.78	29.43
Al	58.2	0.0268	0.0119	1.64	0.92	0.7269	5.99	1.58	1.71
Si	106.7	0.0515	0.0229	2.83	1.52	0.8091	10.35	2.75	2.91
Ag	50.7	0.0811	0.0361	4.88	0.68	0.7398	6.94	4.68	5.09
Au	1.6	0.0794	0.0353	6.75	0.52	0.5233	2.49	5.14	8.37
		1.0000	0.4453	100.00	100.00				

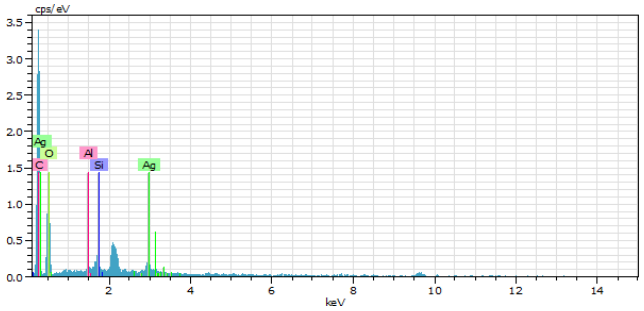

Figure 24. EDX analysis of polyester modified with 45 mL of $AgNO_3$, 6 gr of silitin N85 and 45-min UV irradiation

EDX diffract grams recorded for nanocomposites, polyester fabric and impregnated polyester fabric. Successful coating of the fabric with nanocomposite particles with an average size of 60 nm are uniformly distribute on the surface of the treated fabric. Regarding to the untreated polyester EDX results, two symmetrical peaks are observed at 0.25 = 500 and 0.5 = 4000 which are attributed to C and O species in structure of polyester fabrics (Fig 22). In addition, compared with the above results some distinct are appeared at the EDX results of polyester impregnated with nano composite which are corresponding to silica (1.6 = 600, 1.8 = 1200, 2.2 = 600) and $AgNo_3$ (3 = 500) for silica/kaolinite (fig23).

Structure information obtained from FTIR spectra

The FTIR analysis was performed on polyester fabric impregnated with silica/Kaolinite/silver and as prepared three-component powder (See, fig. 24). The results confirm that the nanocomposite was impregnated on the polyester fabric via in situ method.

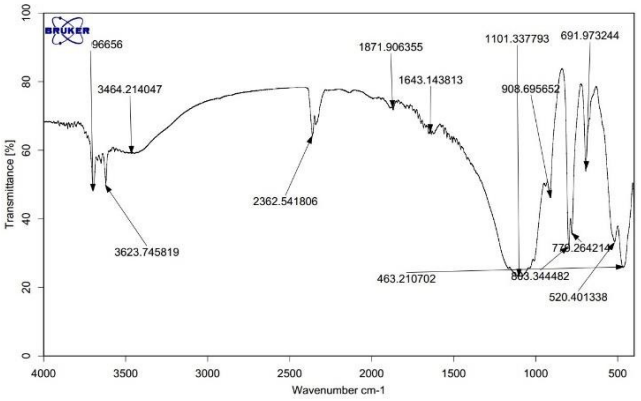

Figure 25. The FTIR spectra of the silica/kaolinite/silver nanocomposite

Figure 25 shows Infrared spectrum of nanocomposite which is exposed to UV light radiation. The peaks centered at 1101, 778 and 691 wave numbers correspond to the siloxane (Si-O-Si) and hydroxyl (Si-O-Al) groups on the surface and aluminum bands, oxygen bands at the layers of Kaolinite/silica particles (in the form of strong tensile) and also bending broadband [111], respectively. The results indicate bending vibrational and tensile modes of absorbed water molecules at the intermediate layers of Kaolinite which are appeared at 3464, 1643 and 463 wave numbers. Moreover, 3623 wave number refers to OH- tensile vibrations mode [112], on the outer and inner surfaces of solid network.

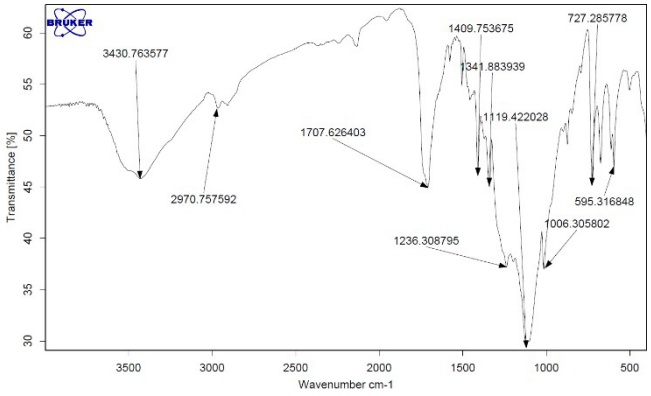

Figure 26. The FTIR spectra of the unmodified polyester

Figure 26 illustrates infrared spectrum of the raw polyester fabric. The C = O ester groups are associated with two extra stereonic group peaks which are located at 1231 and 1006 wave numbers. Also, the short band (1341) should be related to the vibrational state of CH_2 [110,112].

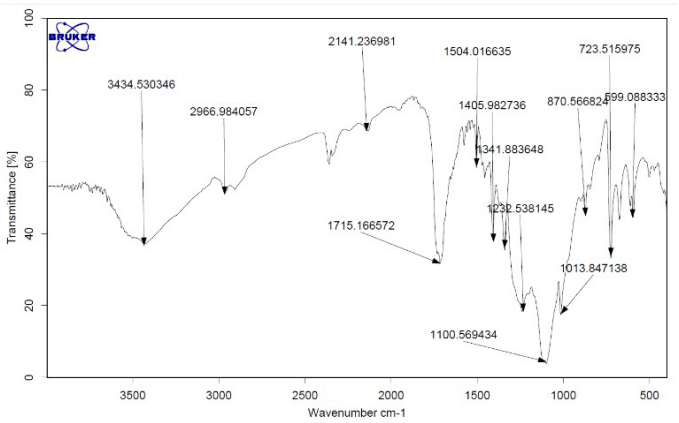

Figure 27. The FTIR spectra of polyester modified with the silica/kaolinite/silver nanocomposite (conditions: 60 mL of $AgNO_3$, 3 gr of silitin N85 and 30-min UV irradiation)

Infrared spectrum of in-situ impregnated polyester fabric given in Figure 27 reveals the presence of siloxane (Si-O-Si) and hydroxyl (Si-O-Al) groups on the surface and aluminum bands, oxygen bands at the layers of Kaolinite/silica particles in the form of strong tensile and also bending broadband which are located at 1013, 699, and 723 wave numbers, respectively [110]. The peaks centered at 2966 and 1715 wave numbers correspond to the bending and tensile modes of absorbed water molecules at the intermediate layers of Kaolinite. Moreover, 3430 band refers to OH- tensile vibrations on the outer and inner surfaces of solid network. Two relatively sharp peaks located at 870 and 1100 [110-112] wavenumbers correspond to the symmetrical tension of Si-O-Si groups appeared after polyester fabric coating under UV light.

Evaluation of electromagnetic properties of the impregnated polyester fabrics

Global efforts in recent years regarding effective protection have resulted in a number of national and international regulations and standards. These specify permissible limit values for power density as well as the electrical and magneticfield strengths for various frequency ranges and signal shapes (Freeden, 2005). It is very important to the people working in areas exposed to electromagnetic fields that the safety procedures used are effective. An electromagnetic field (also EMF or EM field) is a physical field produced by electrically charged objects. When an EM field is passed through impregnated polyester fabric with nanocomposites, three phenomena are possible including: absorption attenuation, attenuation due to reflection and attenuation due to internal transmission of EM waves. Electromagnetic reflection (EMR) is defined as returned EM waves either on the boundary between two media (surface reflection) or in the interior of a medium (volume reflection), whereas transmission is the passage of electromagnetic radiation through a medium (EMT). Absorption is well known as transformation of the radiant power to another type of energy, usually heat by interaction with matter (Parvinzadeh, 2016). Fig 28 and 29 illustrate EMT and EMR curves for the polyester fabric (RAW) and polyester fabric impregnated by silver/silica/kaolinite particles in the range of 5000–8000 MHz. It can be seen that Raw polyester fabric shows a small fluctuation in transition from 2.5 to 3 dB with the variation of frequency. Reflection curves demonstrated two intense peaks at 5665 and 7141 MHz for Run (12) which became stronger for silica/kaolinite/silver nanocomposites. Transmission curves demonstrated four intense peaks at 6772, 7265, 7509 and 7994 MHz for Run (9).

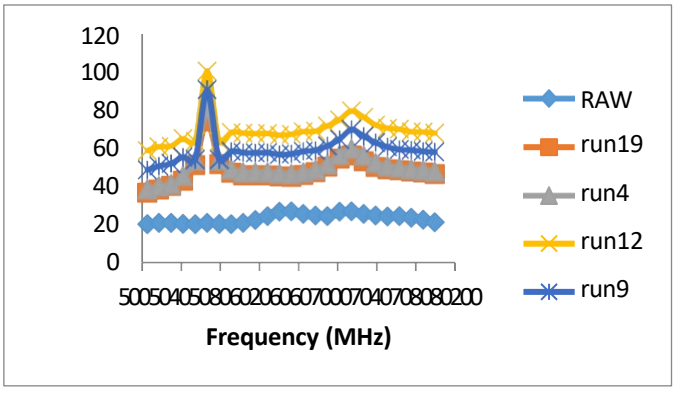

Figure 28. Electromagnetic reflection of polyester fabric and impregnated polyester fabric by nanocomposites

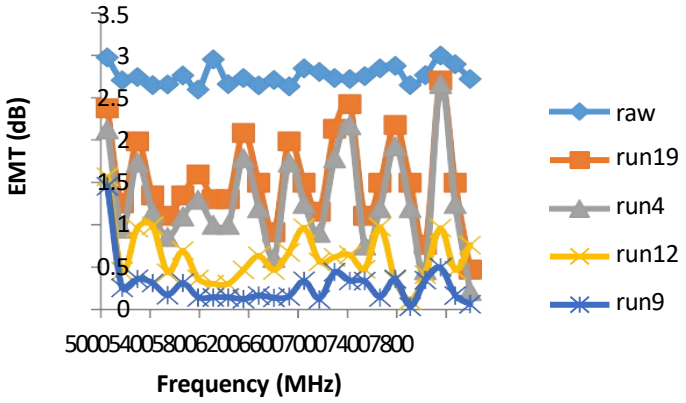

Figure 29. Electromagnetic Transmission of polyester fabric and impregnated polyester fabric by nanocomposites

Analysis of mechanical and magnetic properties of polyester fabric using structural equation modeling

Convergent validity of measurement Models-Convergent validity has been used to fit/examine some available measurement models in the PLS method. The t-statistic and AVE (Average Variance Extracted) are used to examine convergent validity of available measurement models. Then, these measurements are reported and interpreted to get a proper conceptual model.

Table 16. Factor loadings for model structures

Variables	Measure	t statistical	Variable	Measure	t statistical
MS	Fabric	945.675792	CRA	Fabric	1288.46274
	Fabric	3449.37716		Fabric	305.911258
	Fabric	4412.91992		Fabric	507.538789
Air permeability	Fabric (1)	366.217827	strength	Fabric (1)	4635.57751
					2412.35921
	Fabric (2)	116.266273		Fabric (3)	880.464138
					1570.26263
	Fabric (3)	345.046917		Fabric (2)	4635.57751
					2412.35921
Friction	Fabric	1112.33102	Thickness	Fabric	115.509623
	Fabric	582.932893		Fabric	221.617706
	Fabric	214.806093		Fabric	459.154801
Bending	Fabric	1046.25626	Drop absorption	Fabric	23019.5924
	Fabric	225.284559		Fabric	13967.1929
	Fabric	1046.25626		Fabric (3)	4570.698026
Abrasion	Fabric	366.217827			
	Fabric	116.266273			
	Fabric	345.046917			

Factor loadings are determined by calculating t -statistics for indices of model General structure. In the event that Gained- value is greater than or equal to 1.96, factor loading is influential and it should be considered in the proposed model; otherwise, we must remove it from the model. SmartPLS software reported t-statistics of the model variables for hidden structures. Table 16 confirms that t-statistics for all of them are acceptable.

Table 17. AVE values for model structures

Variables	AVE Values
MS	0.995373
Air permeability	0.999668
Friction	0.979042
Bending	0.985594
Drop absorption	0.999253
Abrasion	0.963070
CRA	0.980655
Strength	0.994813
Thickness	0.966619

AVE is another convergent validity measurement which represents the amount of variance that is captured by a construct in relation to the amount of variance due to measurement error. Fornell and Larcker [104] proposed AVE measurements for convergent validity, and also confirmed that, an AVE value greater than 0.5 represents an acceptable convergent validity for measurement models. Table 17 shows AVEs which are reported for each model structures.

Discriminant validity of measurement models. In this research, discriminant validity is used to fit measures in the PLS method. Discriminant validity refers to low correlation between measurements of a hidden variable and an unrelated variable (Henseler, 2015) Discriminant validity in PLS method is measured with two forms: 1) Cross loadings method; 2) Fornell and Larcker [105] criterion which we used in our study.

Discriminant validity is acceptable when AVE values of each structure are greater than shared variance between different structures of the model (i.e., the squared correlation coefficient between structures). Accordingly, an acceptable discriminant validity suggests that, structure is highly correlated in its own indicators than that of other structures. PLS method uses a matrix containing correlation coefficients between the structures, where main diagonal shows the square root of AVE values for each structure.

Table 18. Discriminant validity measurement matrix

values	Ab	Ai	Be	CR	fr	Dr	S	ren	ck
abrasion	1								
Air permeability	0.469731	1							
Bending	0.138491	-0.100677	1						
CRA	0.622068	0.295448	-0.350953	1					
Friction	-0.523711	-0.302584	0.007917	-0.182025	1				
Drop absorption	-0.138456	0.061267	0.131707	-0.381352	0.299581	1			
MS	0.737482	0.063299	0.270056	0.413999	-0.363553	-0.126075	1		
Strength	0.222972	0.103368	0.098939	-0.347277	-0.512697	0.207438	0.154068	1	
Thickness	-0.234947	-0.073096	0.33046	-0.322545	-0.002387	-0.166935	-0.280577	0.224365	1

As shown in Table 18, the square root of AVE values for each structure (main diagonal) is greater than that of its correlation with other structures. This result indicates that discriminant validity of the model measurements is acceptable.

Structural model fit

Coefficient of determination (denoted R^2) is the proportion of the variance in the dependent variable that is predictable from the independent variable. It should be noted that R^2 is determined only for the endogenous variables of the model and it is equal to zero for exogenous structures. Greater values for R^2 (related to intrinsic variables), leads to better fitting model. Chin et.al [106] recommended R^2 values of about 0.67, 0.33and 0.19 using coefficient of determination, which are related to substantial, moderate, and weak fits of structural part of the model, respectively.

Table 19. The coefficients of determination reported for the model's endogenous structures

Variables	Indicator R^2
MS	0.808019
Air permeability	0.277121
Friction	0.441624
Bending	0.343702
Drop absorption	0.248181
Abrasion	0.676020
CRA	0.560717
Strength	0.624695
Thickness	0.361268

According to table 19, magnetic saturation, abrasion and strength have substantial coefficients of determination. The variables consist of bending; crease recovery and thicknesses have moderate coefficients of determination. Hydrophobicity and air permeability have weak coefficients of determination, as well.

Q^2 measure

Q^2 measuring proposed by Stone et al [107], and determines predictive power of the model. They proved that models with an acceptable structural part should be capable of predicting the indices of endogenous variables. When Q^2 values for an endogenous structure are smaller than or equal to zero, the relationships between other structures and endogenous structure are not well-defined. Therefore, the model needs some corrections. Fricker et al. [108] proposed three values of 0.02, 0.15, and 0.35 for power of prediction of endogenous structures. They confirmed, when Q^2 values for an endogenous structure is about 0.02, the model has a weak predictive power. Table 20 shows the Q^2 values for all endogenous variables.

Table 20. Q^2 values for the model's endogenous structures

Variables	Indicator Q^2
MS	0.998453
Air permeability	0.999889
Friction	0.992915
Bending	0.995151
Drop absorption	0.999751
Abrasion	0.987377
CRA	0.993467
Strength	0.999132
Thickness	0.988619

According to Table 20, Q^2 values are in the range (0.987377 into 0.999889) for all kind of model's endogenous structures. Results represent a perfect fitting for the structural model. In the other hand, model shows a substantial predictive power.

Redundancy measurements

This measuring method can be found by multiplying the shared values of structures and their respective R^2 values which indicates degree of variability for the indices of an endogenous structure affected by one or more exogenous structures. No acceptable level is defined for this measurement and then higher values represent better fitting (see, Table 21).

Table 21. Redundancy measure for the model's endogenous structures

Variables	Redundancy indicator
MS	-0.000197
Air permeability	0.057778
Friction	0.068486
Bending	0.009694
Drop absorption	0.040760
Abrasion	0.213017
CRA	0.085272
Strength	0.057755
Thickness	-0.035409

Overall fit of the model

The overall model is composed of both parts of measurement and structural models. So, when its fitness is confirmed, evaluation of model fitness is completed. As mentioned above, only GOF measurement is used to evaluate overall fit of the model.

GOF refers to the overall fitness of structural equation models. Using this method, researchers can evaluate correctness and also check data fitting of the proposed conceptual model. The GOF measurement is developed by Olivares et al [109] which can calculate by following Equation number (11).

$$\text{Gof} = \sqrt{\text{communalities} \times R^2} \quad (11)$$

Olivares et al. (Olivares, 2010) introduced three values of 0.01, 0.25 and 0.36 as weak, moderate and substantial values for GoF measurement, respectively. Table 22 shows the overall fit for all model's endogenous structures which calculated by GOF measurement. Based on results in Table 22, Gof value for all of models was about 0.9848.

Table 22. Overall fit for the model's endogenous structures

Variables	indicator GOF
MS	0.995373
Air permeability	0.999668
friction	0.979042
Bending	0.985594
Drop absorption	0.999253
Abrasion	0.963070
CRA	0.980655
Strength	0.994813
Thickness	0.966619

Hypothesis testing

The most basic measurement to determine the relationship between the structures in the structural equation models is t-statistic. When t-statistic falls outside the interval -1.96 to +1.96, hypothesis is significant at 95% confidence level. Otherwise, estimated path coefficient is not significant and hypothesis is not acceptable. Figure 30 shows conceptual model for the present study in the case of significant coefficients.

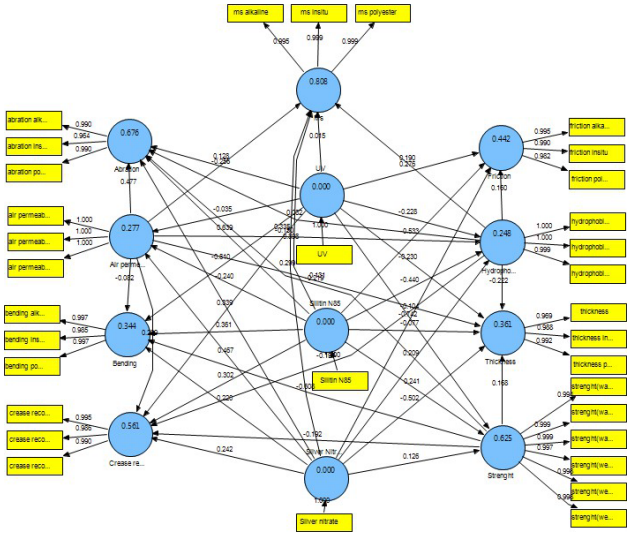

Figure 30. Conceptual model in the case of significant coefficients

Figure 31 illustrates the conceptual model in case of estimating standard coefficients. The figure reveals the extent of variables which have a mutual effect. In a structural equation model, direct effect refers to a correlation between an independent and a dependent variable. Simultaneously, in another direct effect, a dependent variable can be independent, and contrariwise.

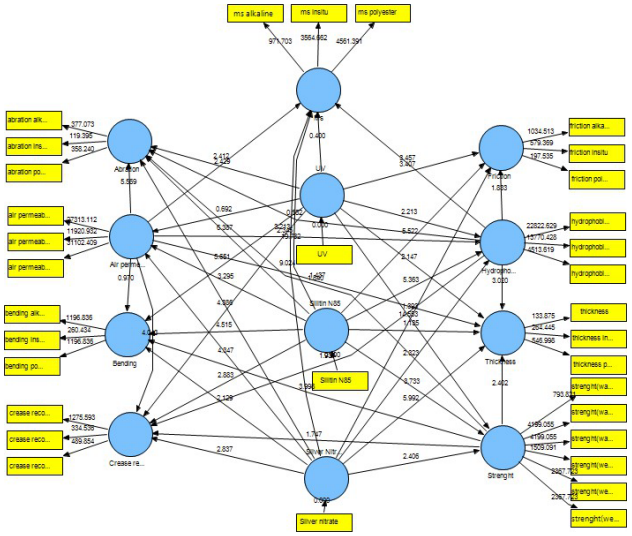

Figure 31. Conceptual model in the case of estimating standard coefficients

The model variables are divided into two types, namely endogenous or downstream, and exogenous or upstream. Each variable in the structural equation modeling system can be considered as an endogenous or an exogenous variable. Endogenous variable is influenced by other variables of the model. In contrast, exogenous variable is not affected by other variables which are available in the model.

Table 23. Final results of hypothesis testing

Test relationship	Impact	t-value	Hypothesis
Air permeability=> Abrasion	0.471967	5.540352	Accepted
Air permeability=> Bending	-0.082220	0.924091	Rejected
Air permeability=> CRA	0.327976	4.111851	Accepted
Air permeability=>	-0.149803	2.271497	Accepted
Air permeability=> Ms	0.099734	2.356592	Accepted
Air permeability=>	0.164727	1.399204	Rejected
Hydrophobia=>Abrasion	0.031746	0.549805	Rejected
Hydrophobia=>CRA	-0.196636	1.918160	Rejected
Hydrophobia=> Friction	0.160064	1.808964	Rejected
Hydrophobia=> Ms	0.190303	3.350671	Accepted
Hydrophobia=> Thickness	-0.222429	3.003157	Accepted
Strength=> Abrasion	-0.219227	1.808524	Rejected
Strength=> Bending	-0.608323	3.790874	Accepted
Strength=> CRA	-0.192287	1.652307	Rejected
Strength=> Thickness	0.168022	2.270842	Accepted
Silitin N85=>Abrasion	0.458587	6.052529	Accepted
Silitin N85=>Air	-0.240398	3.170337	Accepted
Silitin N85=>Bending	0.234069	4.195176	Accepted
Silitin N85=> CRA	0.263570	2.639401	Accepted
Silitin N85=>Friction	-0.598085	5.291811	Accepted
Silitin N85=>Hydrophobia	-0.403755	5.291412	Accepted
Silitin N85=>Ms	0.789962	19.463976	Accepted
Silitin N85=>Strength	0.240872	3.405603	Accepted
Silitin N85=>Thickness	0.022149	1.021551	Rejected
Silver Nitrate=> Abrasion	0.538493	4.274113	Accepted
Silver Nitrate=> Air	0.467024	4.617812	Accepted
Silver Nitrate=> Bending	0.105186	2.090401	Accepted
Silver Nitrate=> CRA	0.330297	2.872964	Accepted
Silver Nitrate=> Friction	-0.081754	1.386645	Rejected
Silver Nitrate=>	0.138555	2.214128	Accepted
Silver Nitrate=> Ms	0.385379	8.618208	Accepted
Silver Nitrate=> Strength	0.126151	2.464500	Accepted
Silver Nitrate=> Thickness	-0.450738	5.345494	Accepted
UV=> Abrasion	-0.116619	2.314356	Accepted
UV=> Air permeability	-0.034906	0.693250	Rejected
UV=> Bending	-0.355572	5.520325	Accepted
UV=> Crease recovery	0.510903	2.775249	Accepted
UV=> Friction	0.239910	3.297624	Accepted
UV=> Hydrophobia	-0.223032	2.426346	Accepted
UV=> Ms	-0.032312	0.399620	Rejected
UV=> Strength	-0.742133	14.292592	Accepted
UV=> Thickness	-0.309720	2.174365	Accepted

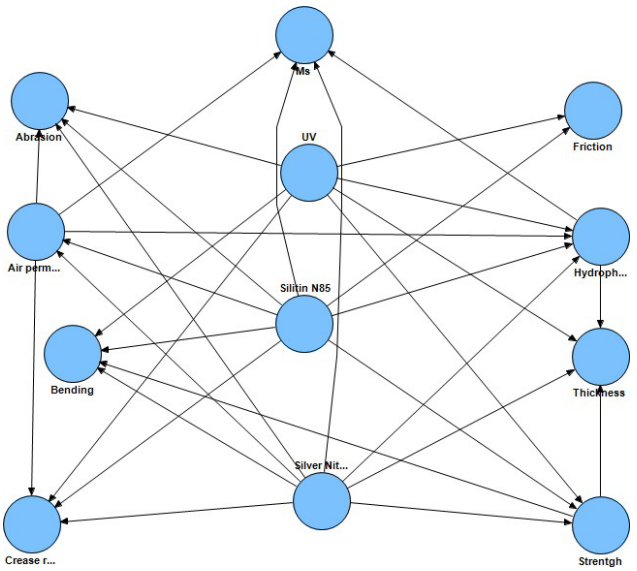

Figure 32. Final structural model of the effects of magnetic saturation and mechanical properties on the polyester fabric impregnated with nanocomposite.

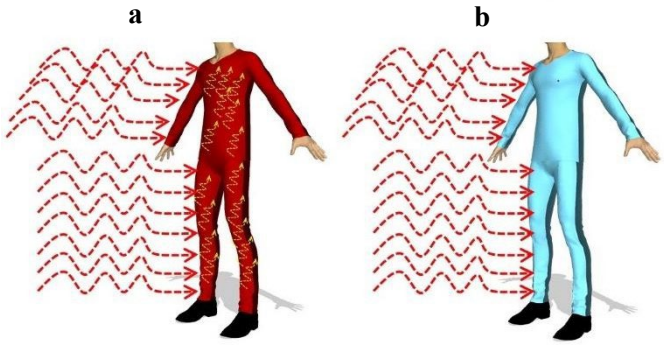

Figure 33. (a) apparel without EM waves protection fabric, (b) apparel with EM waves protection fabric

As shown in table 23, by comparing with t-statistics along with a critical value of about 1.96, 11 hypotheses were rejected and the rest of them were accepted at 95% confidence level.

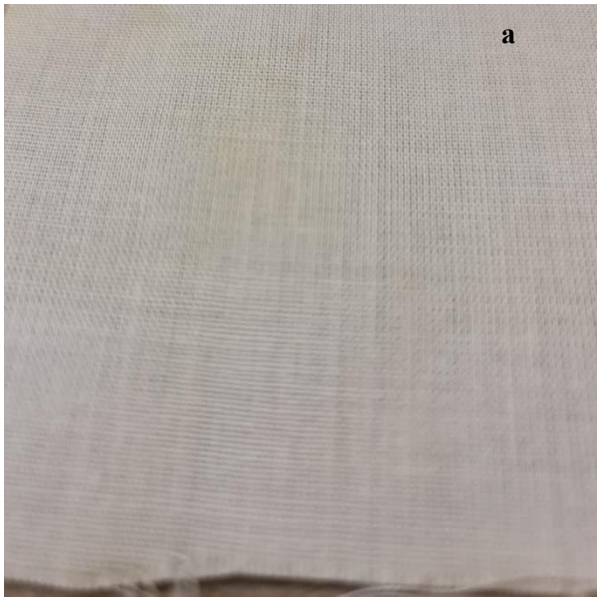

Figure 34. Final products, (a) final coated fabric, (b) final fabric layered in the garment

3. CONCLUSION

Here, 20 characteristic values of silica/Kaolinite/silver nanocomposite were optimized for polyester fabric coating. Designed copies were all in-situ impregnated on the olyester fabric. Physical/chemical properties of as-prepared pure and modified nanocomposites were investigated using MAPPING/EDX and FESEM and FTIR analysis. Moreover, FESEM and Mapping images revealed the presence of nanoparticles on the polyester fabric. EDX and FTIR analyzes also confirmed that nanocomposite particles were impregnated on the polyester fabric. This research done tochange the performance of the polyester fabric by using the nano composite. The experimental results from magnetic saturation test indicated that the optimized nanocomposite can increase magnetic saturation up to 41.559E-3 (emu / gr). Silica and Kaolinite can maintain magnetic property after being placed under a magnetic field. So, these minerals can increase the magnetic saturation by attaching silver along with combining in-situ polyester fabric. Optimized Polyester fabrics, depending on coating materials, can increase their mechanical properties which is very useful for producing the garments and apparel. After impregnation of polyester fabrics, some properties like thickness, strength, abrasion resistance, water permeability, bending and CRA were enhanced. It can affect the fabric comfort because of this fabric can use for formal apparels so these results showed that comfort system of the fabrics were accepted. In addition, UV light exposure time have a significant effect on reducing fabric friction. With

increasing in silver nitrate content, air permeability and bending increased which can enhance comfortability. These properties can be fine for making special clothes with comfort properties to protect the people body from EMP, EMR and EMT waves. Furthermore, using statistical software to forecast the variables effects on each other is very important because researchers can get help and understand their situation and terms of the materials. PLS- SEM is one of the best statistical software which can do it very well. In this research results showed that chemical and textile engineering can use the software very easy to check and improve the researcher's job. This solution will make the way of the projects in the industrial sizes easier.

Funding

The author(s) received no financial support for the research, authorship, and/or publication of this article.

REFERENCES

[1] Idris SA, Harvey SR, Gibson LT. Selective extraction of mercury (II) from water samples using mercapto functionalised-MCM-41 and regeneration of the sorbent using microwave digestion. Journal of hazardous materials. 2011 Oct 15;193:171-6.

[2] Jiang B, Chen Z, Sun Y, Yang H, Zhang H, Dou H, Zhang L. Fabrication of superhydrophobic cotton fabrics using crosslinking polymerization method. Applied Surface Science. 2018 May 31;441:554-63.

[3] Prasad V, Arputharaj A, Bharimalla AK, Patil PG, Vigneshwaran N. Durable multifunctional finishing of cotton fabrics by in situ synthesis of nano-ZnO. Applied Surface Science. 2016 Dec 30;390:936-40.

[4] Li D, Guo Z. Versatile superamphiphobic cotton fabrics fabricated by coating with SiO2/FOTS. Applied Surface Science. 2017 Dec 31;426:271-8.

[5] Lei Y, Cai W, Wilde G. Highly ordered nanostructures with tunable size, shape and properties: A new way to surface nano-patterning using ultra-thin alumina masks. Progress in Materials Science. 2007 May 1;52(4):465-539.

[6] Mallakpour S, Naghdi M. Polymer/SiO2 nanocomposites: Production and applications. Progress in Materials Science. 2018 Aug 1;97:409-47.

[7] Dominguez-Benetton X, Varia JC, Pozo G, Modin O, Ter Heijne A, Fransaer J, Rabaey K. Metal recovery by microbial electro-metallurgy. Progress in Materials Science. 2018 May 1;94:435-61. Ojijo V, Ray SS. Nano-biocomposites based on synthetic aliphatic polyesters and nanoclay. Progress in Materials Science. 2014 May 1;62:1-57.

[8] Wanga X., Ding B., Sun G., Wang M., Yu J. (2013). Electro-spinning/netting: A strategy for the fabrication of three-dimensional polymer nano-fiber/nets. Progress in Materials Science, 58, 1173–1243.

[9] Selim MS, Shenashen MA, El-Safty SA, Higazy SA, Selim MM, Isago H, Elmarakbi A. Recent progress in marine foul-release polymeric nanocomposite coatings. Progress in Materials Science. 2017 Jun 1;87:1-32.

[10] Joshi M, Adak B, Butola BS. Polyurethane nanocomposite based gas barrier films, membranes and coatings: A review on synthesis, characterization and potential applications. Progress in Materials Science. 2018 Aug 1;97:230-82.

[11] Majdzadeh-Ardakani K, Holl MM. Nanostructured materials for microwave receptors. Progress in Materials Science. 2017 Jun 1;87:221-45.

[12] Bai RG, Ninan N, Muthoosamy K, Manickam S. Graphene: a versatile platform for nanotheranostics and tissue engineering. Progress in Materials Science. 2018 Jan 1;91:24-69.

[13] Wang JG, Kang F, Wei B. Engineering of MnO2-based nanocomposites for high-performance supercapacitors. Progress in Materials Science. 2015 Oct 1;74:51-124.

[14] Karger-Kocsis J, Mahmood H, Pegoretti A. Recent advances in fiber/matrix interphase engineering for polymer composites. Progress in Materials Science. 2015 Aug 1;73:1-43.

[15] Leng J, Lan X, Liu Y, Du S. Shape-memory polymers and their composites: stimulus methods and applications. Progress in Materials Science. 2011 Sep 1;56(7):1077-135.

[16] Oliveux G, Dandy LO, Leeke GA. Current status of recycling of fibre reinforced polymers: Review of technologies, reuse and resulting properties. Progress in materials science. 2015 Jul 1;72:61-99.

[17] Wu R, Zhou K, Yue CY, Wei J, Pan Y. Recent progress in synthesis, properties and potential applications of SiC nanomaterials. Progress in Materials Science. 2015 Jul 1;72:1-60.

[18] Bourmaud A, Beaugrand J, Shah DU, Placet V, Baley

[19] C. Towards the design of high-performance plant fibre composites. Progress in Materials Science. 2018 Aug 1;97:347-408.

[20] George M, Chae M, Bressler DC. Composite materials with bast fibres: Structural, technical, and environmental properties. Progress in materials Science. 2016 Oct 1;83:1-23.

[21] Ramesh M. Fiber based bio-materials: A review on processing and properties. Progress in Materials Science. 2016;78-79:1–92.

[22] Hanus MJ, Harris AT. Nanotechnology innovations for the construction industry. Progress in Materials Science. 2013;58:1056–1102.

[23] Krol P. Synthesis methods, chemical structures and phase structures of linear polyurethanes. Properties and applications of linear polyurethanes in polyurethane elastomers, copolymers and ionomers. Progress in Materials Science. 2007;52:915–1015.

[24] Lancry M, Régnier E, Poumellec B. Fictive temperature in silica-based glasses and its application to optical fiber manufacturing. Progress in Materials Science. 2012;57:63–94.

[25] Lisjak D, Mertelj A. Anisotropic magnetic nanoparticles: A review of their properties, syntheses and potential applications. Progress in Materials Science. 2018;95:286–328.

[26] Franco V, Blázquez JS, Ipus JJ, Law JY, Moreno- Ramírez LM, Conde A. Magneto caloric effect: From materials research to refrigeration device. Progress in Materials Science. 2018;93:112–232.

[27] Xu S, Habib AH, Peakel AD, McHenry ME. Magnetic nanoparticle-based solder composites for electronic packaging applications. Progress in Materials Science. 2015;67:95–160.

[28] Stocks GM, Eisenbach M, Ujfalussy B, Lazarovits B, Szunyogh L, Weinberger P. On calculating the magnetic state of nanostructures. Progress in Materials Science. 2007;52:371–387.

[29] Song C, Cui B, Li F, Zhou X, Pan F. Recent progress in voltage control of magnetism: Materials, mechanisms, and performance. Progress in Materials Science. 2017;87:33–82.
[30] Krajina BA, Proctor AC, Schoen AP, Spakowitz AJ, Heilshorn SC. Biotemplated synthesis of inorganic materials: An emerging paradigm for nanomaterial synthesis inspired by nature. Progress in Materials Science. 2018;91:1–23.
[31] Zieliński M, Rusanowska P, Dębowski M, Hajduk A. Influence of static magnetic field on sludge properties. Science of the Total Environment. 2018;625:738–742.
[32] Smarzewska S, Mie˛ko E, Guziejewski D, Zieliński M, Burnat B. Graphene oxide activation with a constant magnetic field. Analytical Chemical Acts. 2018;1011:35–39.
[33] Billoir P. Correcting a magnetic field map through the alignment of tracks. Nuclear Instruments and Methods in Physics Research. Accepted 12 June 2018.
[34] Chen Q, Shen H. Numerical study on solidification characteristics under pulsed magnetic field. Heat and Mass Transfer. 2018;120:997–1008.
[35] Basant KJ, Babatunde A. Impact of induced magnetic field on magneto hydrodynamic (MHD) natural convection flow in a vertical annular micro-channel in the presence of radial magnetic field. Propulsion and Power Research. Accepted 20 September 2017.
[36] Kohyani MT, Ghasemi B, Raisi A, Aminossadati SM. Melting of cyclohexane–Cu nano-phase change material (nano-PCM) in porous medium under magnetic field. Taiwan Institute of Chemical Engineers. 2017;77:142–151.
[37] Chunga JY, Leea JG, Baeka YK, Shinb PW, Kima YK. Magnetic field-induced enhancement of thermal conductivities in polymer composites by linear clustering of spherical particles. Composites Part B. 2018;136:215–221.
[38] Dong Y, Wu B, Wang M, Xiao H, Xiao S, Sun C, Li H, Jian S. Magnetic field and temperature sensor based on D-shaped fiber modal interferometer and magnetic fluid. Optics and Laser Technology. 2018;107:169–173.
[39] Maa WT, Kumara SR, Hsua CT, Shiha CM, Tsaib SW, Yangc ChCh, Liud YL, Luea ShL. Magnetic field-assisted alignment of graphene oxide Nano sheets in a polymer matrix to enhance ionic conduction. Membrane Science. 2018;563:259–269.
[40] Hongkun Zh, Hongming H, Xiuguang W, Zhongyi L, Bo D, Hanwen Y. Four unprecedented 2D trinuclear Mn(II)-complexes with adenine nucleobase controlled by solvent or co-ligand: Hydrothermal synthesis, crystal structure and magnetic behavior. Molecular Structure. 2018;1155:687–694.
[41] Yang Y, Wang W, Lv D, Liu J, Gao Zh, Wang Ze, Carlo M. Study of magnetic behaviors in a quadrangle ferromagnetic using Nano island. Physics and Chemistry of Solids. 2018;120:109–122.
[42] Rout J, Choudhary RNP. Structural, electrical and magnetic behavior of mechano-thermally synthesized multi-doped bismuth ferrite. Ceramics International. 2018;44:11543–11553.
[43] Bangruwaa JS, Vashisth BK, Singh N, Vermab V. Anomalous ferroelectric and magnetic behavior in BPFO-NZFO multi-ferroic nano-composites. Ceramics International. 2018;44:11737–11744.
[44] Wanga WM, Liu SY, Xu M, Bai L, Wang HQ, Wena X, Zhao XY, Qiao H, Wua Zh. Structures and magnetic properties of phenoxo-O-bridged dinuclear lanthanide(III) compounds: Single-molecule magnet behavior and magnetic refrigeration. Polyhedron. 2018;145:114–119.
[45] Malewski S, Malkemper EP, Sedláček F, Šumberac R, Caspar K, Burda H, Begall S. Attracted by a magnet: Exploration behavior of rodents in the presence of magnetic objects. Behavioral Processes. 2018;151:11– 15.
[46] Sokolova IL, Cherkasova VR, Vasilyeva AV, Bragina VA, Nikitin MP. Paramagnetic colloidal ferrihydrite nanoparticles for MRI contrasting. Colloids and Surfaces A. 2018;539:46–52.
[47] Ravera E, Parigi G, Luchinat C. Perspectives on paramagnetic NMR from a life sciences infrastructure. Magnetic Resonance. 2017;282:154–169.
[48] Noori A, Mostajaboddavati M, Ziaie F. Retrospective dosimetry using fingernail electron paramagnetic resonance response. Nuclear Engineering and Technology. 2018;50:526–530.
[49] Xiang Y, Xia Q, Luo J, Liu Y, Peng Y, Wang D, Nie Y, Guo G. Observation of ferromagnetism in black phosphorus nanosheets with high magnetization by liquid exfoliation. Solid State Communications. Accepted 18 June 2018.
[50] Miao Y, Qiu Sh, Zhang G, Ren J, Wang Ch, Hu G. Polarons in organic ferromagnets. Organic Electronics. 2018;55:133–139.
[51] Zhou D, Chang X, Hed Y, Wang H, Cao P, Yang L. Influence of key factors on Eddy current testing sensitivity and monotonicity on subsurface depth for ferromagnetic and non-ferromagnetic materials. Sensors and Actuators A. 2018;278:98–110.
[52] Watarai H, Fan R, Liu JY, Djauhari J. Falling velocity magnetometry of ferromagnetic micro particles. Magnetism and Magnetic Materials. 2018;462:22–28.
[53] Jungfleisch MB, Zhang W, Hoffmann A. Perspectives of antiferromagnetic spintronic. Physics Letters A. 2018;382:865–871.
[54] Paul C, Lou A, Kumar S. Spin-Hall effect and emergent antiferromagnetic phase transition in n-Si. Magnetism and Magnetic Materials. 2018;452:129–133.
[55] Kozub VI, Muradov MI, Galperin YM. Electron drag in ferromagnetic structures separated by an insulating interface. Magnetism and Magnetic Materials. 2018;456:257–262.
[56] Shakil M, Husain A, Zafar M, Ahmad Sh, Khan MI, Masood MK, Majid A. Ferromagnetism in GaN doped with transition metals and rare-earth elements: A review. Chinese Journal of Physics. Accepted 21 May 2018.
[57] Yang G, Wu Y, Ma Sh, Fu Y, Gao D, Zhang Zh, Li J. Defect-induced room temperature ferromagnetism in silicon carbide nanosheets. Superlattices and Microstructures. 2018;119:19–24.
[58] Dhar V, Provino A. Ferromagnetism in the orthorhombic PrPd and SmPd. Alloys and Compounds. 2018;762:254–259.
[59] Yoon S, Son K, Ebbinghaus SG, Widenmeyer M, Weidenkaff A. Ferromagnetism in nitrogen and fluorine substituted BaTiO3. Alloys and Compounds. 2018;749:628–633.
[60] Guyader JL, Totaro N, Maxit L. Statistical Energy Analysis with fuzzy parameters to handle populations of structures. Sound and Vibration. 2016;379:119– 134.
[61] Molina M, Mota M, Ramos A. Statistical inference in two-sex biological populations with reproduction in a random

environment. Ecological Complexity. 2017;30:63–69.
[62] Greenberg L, Jairath V, Pearse R, Kahan BC. Pre-specification of statistical analysis approaches in published clinical trial protocols was inadequate. Clinical Epidemiology. Accepted 25 May 2018.
[63] Xia Y, Sun J. Hypothesis testing and statistical analysis of microbiome. Genes & Diseases. 2017;4:138–148.
[64] Saleh TA, Adio SO, Asif M, Dafalla H. Statistical analysis of phenols adsorption on diethylenediamine modified activated carbon. Cleaner Production. 2018;182:960–968.
[65] Reid N. Statistical science in the world of big data. Statistics and Probability Letters. 2018;136:42–45.
[66] Qianchuan H, Yang L, Wei S. Statistical analysis of non-coding RNA data. Cancer Letters. 2018;417:161– 167.
[67] Zhang F, Tony HK, Shi Y. Bayesian duality and risk analysis on the statistical manifold of exponential family with censored data. Computational and Applied Mathematics. 2018;342:534–549.
[68] Nayak P, Mukherjee AK, Pandit E, Pradhan SK. Application of Statistical Tools for Data Analysis and Interpretation in Rice Plant Pathology. Rice Science. 2018;25(1):1–18.
[69] Schubring S, Lorscheid I, Meyer M, Ringle CM. The PLS agent: Predictive modeling with PLS-SEM and agent-based simulation. Business Research. 2016;69:4604–4612.
[70] Shmueli G, Ray S, Estrada JMV, Chatla SB. The elephant in the room: Predictive performance of PLS models. Business Research. 2016;69:4552–4564.
[71] Schlittgen R, Ringle CM, Sarstedt M, Becker JM. Segmentation of PLS path models by iterative reweighted regressions. Business Research. 2016;69:4583–4592.
[72] Li Q, Pan F, Zhao Z. Concurrent probabilistic PLS regression model and its applications in process monitoring. Chemometrics and Intelligent Laboratory Systems. 2017;171:40–54.
[73] Mahanty B. Alternate deflation and inflation of search space in reweighted sampling: An effective variable selection approach for PLS model. Chemometrics and Intelligent Laboratory Systems. 2018;174:45–55.
[74] Becker JM, Ismail IR. Accounting for sampling weights in PLS path modeling: Simulations and empirical examples. European Management Journal. 2016;34:606–617.
[75] Flyborg L, Björlenius B, Ullner M, Persson KM. A PLS model for predicting rejection of trace organic compounds by Nano filtration using treated wastewater as feed. Separation and Purification Technology. 2017;174:212–221.
[76] Wang Q, Zhou W, Cheng Y, Ma G, Chang X, Miao Y, Chen E. Regularized moving least-square method and regularized improved interpolating moving least-square method with nonsingular moment matrices. Applied Mathematics and Computation. 2018;325:120–145.
[77] Xu W, Chen W, Liang Y. Feasibility study on the least square method for fitting non-Gaussian noise data. Physical A. 2018;492:1917–1930.
[78] Beltman R, Boonkkamp JT, IJzerman W. A least- squares method for the inverse reflector problem in arbitrary orthogonal coordinates. Computational Physics. 2018;367:347–373.
[79] Keith B, Petrides S, Fuentes F, Demkowicz D. Discrete least-squares finite element methods. Computer Methods in Applied Mechanics and Engineering. 2017;327:226–255.
[80] Ahmadinia M, Safari Z. Numerical solution of singularly perturbed boundary value problems by improved least squares method. Computational and Applied Mathematics. 2018;331:156–165.
[81] Hendrych R, Cipra T. On conditional covariance modelling: An approach using state space models. Computational Statistics and Data Analysis. 2016;100:304–317.
[82] Tong J, Hu R, Xi J, Xiao Z, Guo Q, Yu Y. Linear shrinkage estimation of covariance matrices using low- complexity cross-validation. Signal Processing. 2018;148:223–233.
[83] Noack B, Sijs J, Reinhardt M, Hanebeck UD. Decentralized data fusion with inverse covariance intersection. Automatica. 2017;79:35–41.
[84] Plake D, Stella P, Moravek A, Mayer JC, Ammann C, Held A, Trebs I. Comparison of ozone deposition measured with the dynamic chamber and the eddy covariance method. Agricultural and Forest Meteorology. 2015;206:97–112.
[85] Connan O, Maro D, Ebert DH, Solier L, Caldeira Ideas P, Laguionie P, St-Amant N. In situ measurements of tritium evapotranspiration (^{3}H-ET) flux over grass and soil using the gradient and eddy covariance experimental methods and the FAO-56 model. Environmental Radioactivity. 2015;148:1–9.
[86] Prajapati P, Santos EA. Estimating methane emissions from beef cattle in a feedlot using the eddy covariance technique and footprint analysis. Agricultural and Forest Meteorology. 2018;258:18–28.
[87] Helene O, Mariano L, Filho ZG. Useful and little-known applications of the Least Square Method and some consequences of covariance's. Nuclear Instruments and Methods in Physics Research A. 2016;833:82–87.
[88] Mou Y, Zhou L, Chen W, Fan J, Zhao X. Maximum correntropy criterion partial least squares. Optik. 2018;165:137–147.
[89] Haeltermana R, Lauwensa B, Utterbeeck FV, Bruyninckx H, Vierendeels J. On the similarities between the quasi-Newton least squares method and GMRes. Computational and Applied Mathematics. 2015;273:25–28.
[90] Peng X, Cai Y, Li Q, Wang K. The least-squares method based on coupling coefficients for reactor power distribution reconstruction. Annals of Nuclear Energy. 2016;94:272–278.
[91] Bocheva P, Gerritsma M. A spectral mimetic least- squares method. Computers and Mathematics with Applications. 2014;68:1480–1502.
[92] Lyons MB, Keith DA, Phinn SR, Mason TJ, Elith J. A comparison of resampling methods for remote sensing classification and accuracy assessment. Remote Sensing of Environment. 2018;208:145–153.
[93] González O, Trinidad JM, Ochoa JAC, Borroto MG. Study of the impact of resampling methods for contrast pattern-based classifiers in imbalanced data bases. Neurocomputing. 2016;175:935–947.
[94] Hilafu H, Wub W. Partial projective resampling method for dimension reduction: With applications to partially linear models. Computational Statistics and Data Analysis. 2017;109:1–14.
[95] Rumpf K, Granitzer P, Poelt P. Non-saturating magnetic behavior of a ferromagnetic semiconductor/metal nanocomposite. Magnetism and Magnetic Materials. 2010;322:1283–1285.

[96] Young HD, Freedman RA, Lewis Ford A. University physics, Standard Edition includes Chapters 1–37. ISBN 13: 978-0-321-69686-1.
[97] Brownlie L, Ostafichuk P, Carboc J, Demarest N. Air permeability of sports fabrics at running speeds. Procedia Engineering. 2014;72:697–702.
[98] Vlad D, Cioca LL. Research regarding the influence of raw material and woven fabric geometry on the air permeability of mattress. Procedia Engineering. 2017;181:324–329.
[99] Zhang H, Wu X, Zhu C, Ming Y, Bi J. Study on down-proofness of down home textile fabrics. Physics Procedia. 2015;25:245–250.
[100] Eltahan E. Structural parameters affecting tear strength of fabric tents. Alexandria Engineering Journal. 2018;57:97–105.
[101] Trabelsi H, Romero E, Jamei M. Tensile strength during drying of remolded and compacted clay: The role of fabric and water retention. Applied Clay Science. 2018;162:57–68.
[102] Seretis GV, Kostazos PK, Manolakos DE. On the strength and failure mechanism of woven para- aramid protection fabrics. Mechanics of Materials. 2016;97:92–99.
[103] Fagone M, Loccarini F, Ranocchiai G. Strength evaluation of jute fabric for the reinforcement of rammed earth structures. Composites Part B. 2017;113:1–13.
[104] Wang XY, Gong RH, Dong Z, Porat I. Abrasion resistance of thermally bonded 3D nonwoven fabrics. Wear. 2007;262:424–43
[105] Henseler J, Ringle CM, Sarstedt M. A new criterion for assessing discriminant validity in variance-based structural equation modeling. Acad Mark Sci. 2015;43:115–35.
[106] Zait A, Bereta EP. Methods for testing discriminant validity. Manag Mark. 2011;11:217–24.
[107] Monecke A, Leisch F. SEM-PLS: Structural Equation Modeling Using Partial Least Squares. J Stat Softw. 2012;48(3):1–32.
[108] Akter S, D'Ambra J, Ray P. An evaluation of PLS based complex models: the roles of power analysis, predictive relevance and GoF index. In: Proceedings of the Seventeenth Americas Conference on Information Systems, Detroit, Michigan; 2011.
[109] Fricker S, Kreisler C, Tan L. An exploration of the application of PLS path modeling approach to creating a summary index of respondent burden. Survey Res Methods – U.S. Bureau of Labor Statistics, 2 Massachusetts Avenue NE, Washington, DC 20212, JSM 2012.
[110] Olivares AM, Forero CG. Goodness-of-Fit Testing. In: International Encyclopedia of Education, 7; 2010. p. 190–6.
[111] Tanja MG, Kristin BA, Ole FN. ATR-FTIR, FT-NIR and near-FT-Raman spectroscopic studies of molecular composition in human skin in vivo and pig ear skin in vitro. J Spectrosc. 2008;22:437–57.
[112] Parvinzadeh MG, Almasian A. Synthesizing tertiary silver/silica/kaolinite nanocomposite using photo-reduction method: Characterization of morphology and electromagnetic properties. J Compos Part B. 2012;43:3374–83.
[113] Chou KS, Ren CY. Synthesis of nanosized silver particles by chemical reduction method. Mater Chem Phys. 2000;6:64–241.
[114] Zarinabadi E, Abghari R, Nazari A, Mirjalili
[115] M. Modeling and optimization of electromagnetic and saturated magnetic properties of polyester fabrics coated with Ag/kaolin/silica nanocomposites. Bulgarian Chem Commun. 2018;50:154–67.
[116] Zarinabadi E, Abghari R, Nazari A, MirjaliliEnvironmental effects of enhancement of mechanical and hydrophobic properties of polyester fabrics using silica/kaolinite/silver nanocomposite: A facile technique for synthesis and RSM optimization. Eurasia J Biosci. 2018;12:437–